

## The Effects of Mountains on the General Circulation of the Atmosphere as Identified by Numerical Experiments

SYUKURO MANABE AND THEODORE B. TERPSTRA

*Geophysical Fluid Dynamics Laboratory/NOAA, Princeton University, Princeton, N. J. 08540*

(Manuscript received 26 June 1973)

### ABSTRACT

In order to identify the effects of mountains upon the general circulation of the atmosphere, a set of numerical experiments is performed by use of a general circulation model developed at the Geophysical Fluid Dynamics Laboratory of NOAA. The numerical time integrations of the model are performed with and without the effects of mountains. By comparing the structure of the model atmospheres that emerged from these two numerical experiments, it is possible to discuss the role of mountains in maintaining the stationary and transient disturbances in the atmosphere.

The model adopted for this study has a global computational domain and covers both the troposphere and stratosphere. For the computation of radiative transfer, the distribution of incoming solar radiation in January is assumed. Over the ocean, the observed distribution of the sea surface temperature of February is assumed as a lower boundary condition of the model. Over the continental surface, temperature is determined such that the condition of heat balance at the ground surface is satisfied. The mountain topography is taken into consideration using the so-called  $\sigma$ -coordinate system in which pressure normalized by surface pressure is used as a vertical coordinate. The grid size for the computation of horizontal finite differences is chosen to be about 250 km. Nine finite-difference levels are chosen in unequal pressure intervals so that these levels can represent not only the structure of the mid-troposphere but also that of the stratosphere and the planetary boundary layer.

The results of the numerical experiments indicate that it is necessary to consider the effects of mountains for the successful simulation of the stationary flow field in the atmosphere, particularly in the upper troposphere and stratosphere. As predicted by Bolin, the flow field in the upper troposphere of the mountain model has a stationary trough in the lees of major mountain ranges such as the Rocky Mountains and the Tibetan Plateau. To the east of the trough, an intense westerly flow predominates. In the stratosphere, an anticyclone develops over the Aleutian Archipelago. These features of the mountain model, which are missing in the model without mountains, are in good qualitative agreement with the features of the actual atmosphere in winter.

In the model troposphere, mountains increase markedly the kinetic energy of stationary disturbances by increasing the stationary component of the eddy conversion of potential energy, whereas mountains decrease the kinetic energy of transient disturbances. The sum of the stationary and transient eddy kinetic energy is affected little by mountains. In the model stratosphere, mountains increase the amplitude of stationary disturbances partly because they enhance the energy supply from the model troposphere to the stratosphere.

According to wavenumber analysis, the longitudinal scale of eddy conversion in the model atmosphere increases significantly due to the effects of mountains. This increase results mainly from the large increase of stationary eddy conversion which takes place at very low wavenumbers.

The results of the analysis reveal other important effects of mountains. For example, the probability of cyclogenesis in the model atmosphere increases significantly on the lee side of major mountain ranges where the core of the westerly jet is located. Also, mountains affect the hydrologic processes in the model atmosphere by modifying the field of three-dimensional advection of moisture, and alter the global distribution of precipitation very significantly. In general, the distribution of the model with mountains is less zonal and more realistic than that of the model without mountains.

### 1. Introduction

The effect orography has upon the stationary, planetary-scale flow field in the atmosphere has been the subject of many studies. Using a one-dimensional, barotropic model, Charney and Eliassen (1949) concluded that the large-scale quasi-stationary disturbances of the middle latitudes are produced mainly by the

forced ascent of the westerly currents over the continental land masses. Bolin (1950) computed the effects of a bell-shape mountain upon large-scale flow with a barotropic model and carried out a comprehensive discussion of the influence of mountains. On the other hand, Smagorinsky (1953) and Döös (1962) evaluated the effects of heat sources and sinks upon stationary flow using a baroclinic model. Both Bolin and Smagorinsky

concluded that the thermal effects account for the essential features of the observed distribution of sea level pressure, whereas the relative importance of mountain effects increases with increasing altitude. More recently, Sankar-Rao and Saltzman attempted to improve these studies by representing the lower boundary conditions with many spherical harmonics and obtained somewhat different results (Sankar-Rao, 1965, 1970; Sankar-Rao and Saltzman, 1969; Saltzman 1968). They concluded that a good deal of the longitudinal variance of the mean tropospheric state in the middle latitudes is explainable by the effects of asymmetric surface heating.

The theoretical studies mentioned above involve many simplifying assumptions. For example, the amplitude of the stationary perturbation is assumed to be small with the result that the interactions among stationary waves and between stationary and transient disturbances were neglected. The zonal current is assumed to be uniform in the meridional direction. Furthermore, the distribution of heat sources is highly idealized. It is probable that the removal of some of these assumptions would significantly alter the results of the theoretical calculations. Therefore, it is desirable to construct a mathematical model of the atmosphere free of these assumptions, and to perform numerical experiments for the satisfactory identification of the role of mountains in maintaining the large-scale stationary flow field.

Many numerical experiments have been made to identify the influence of orography upon the planetary-scale flow field. The work of Mintz and Arakawa (Mintz, 1965) was a first attempt of this kind. They constructed a global model with realistic orography and were successful in simulating remarkably well the distribution of sea-level pressure. The results from the model with realistic mountains were compared with those from the mountainless model. Based on this comparison, Mintz made an interesting suggestion that the Tibetan plateau is responsible for the maintenance of the intense Siberian high during the winter. Unfortunately, the details of this comparison are not available.

In Mintz's model, the effects of the hydrologic cycle on the large-scale flow were not taken into consideration explicitly. Recently, Kasahara and Washington (1971) constructed a multi-level, global general circulation model with moist processes and performed numerical experiments with and without mountains. Based upon the results from these experiments, they concluded that the thermal rather than orographic effects are the dominating factor which determines the stationary flow field in the troposphere. Superficially, their conclusion seems to agree with that of Sankar-Rao and Saltzman (1969). It is not possible, however, to compare these two studies because Kasahara and Washington (1971) did not show the actual structure of stationary disturbances in the upper troposphere.

Kikuchi also investigated the effects of mountains by use of his quasi-geostrophic, two-level spectral model and concluded that the orographic effects primarily determine the large-scale features of the winter circulation (private communication). [See also Kikuchi (1969) for the description of his spectral model.] The details of the results from his numerical experiments are not available to us at the present time.

The review of the preceding studies on this subject seems to indicate that the problem is far from solved. Therefore, it was decided to re-examine the dynamical influence of mountains and heat sources by use of the general circulation model developed at the Geophysical Fluid Dynamics Laboratory of NOAA. The basic strategy of this study was to perform extensive comparisons between the results from the mountain model and those from the mountainless model. Special emphasis of the study was placed upon the re-examination of various theoretical studies in the light of the results from our numerical experiments. The structure and the performance of this version of the global model were reported by Holloway and Manabe (1971), and Manabe *et al.* (1970a). A preliminary report of the mountain study was published earlier by Manabe and Holloway (1970). After this preliminary study was completed, it was found that the results suffer a great deal from the coarseness of the computational resolution of the model. Therefore, the numerical experiments were repeated after halving the grid size of the horizontal finite-differencing scheme from about 500 km to about 250 km. This paper summarizes the results from the numerical experiments by the model with this finer computational resolution.

## 2. Brief description of the model

### a. Model structure

As mentioned in the Introduction, the structure of the global model used for this study was described in detail by Holloway and Manabe (1971). Therefore, only a very brief sketch of the global model is given here.

The primitive equations of motion in the spherical coordinate system are used. The effects of mountains are incorporated by use of the so-called  $\sigma$ -coordinate system proposed by Phillips (1957). The distribution of topography used for this study is shown in Fig. 2.1. In order to simulate the effects of subgrid-scale mixing, a nonlinear viscosity is employed as suggested by Smagorinsky (1963). The finite-difference forms of the dynamical equations and the global grid system are similar to those proposed by Kurihara and Holloway (1967). The horizontal grid size adopted for this study is approximately 250 km. Table 1 indicates the actual grid sizes at various latitudes. In the vertical direction, nine finite-difference levels are chosen so as to represent the structure of the planetary boundary layer as well as that of the stratosphere. The approximate heights

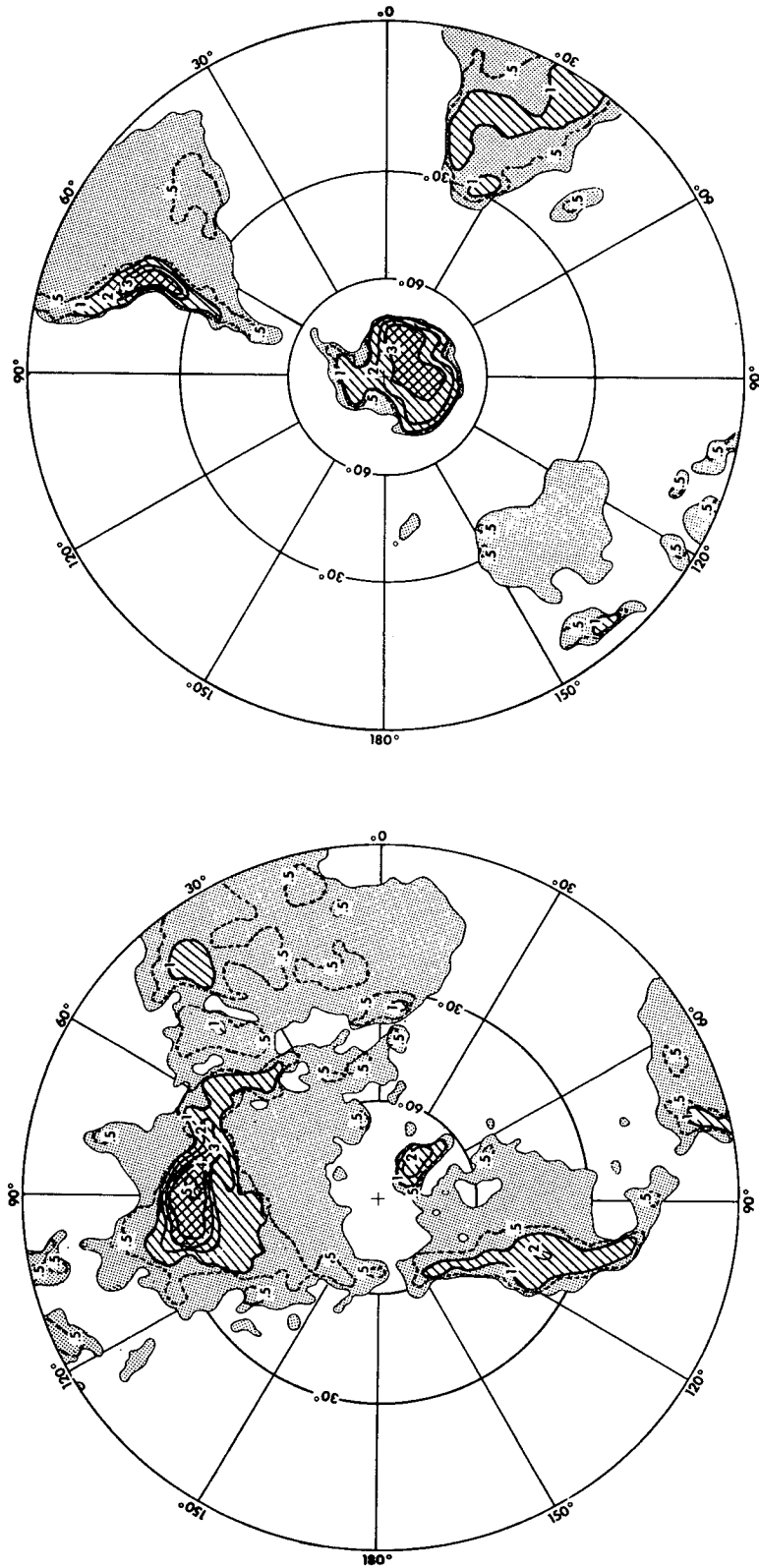


FIG. 2.1. The distribution of topography adopted for the numerical experiments: units, km.

TABLE 1. Grid sizes of the models at selected latitudes. Distances are in kilometers.

Latitude	$\Delta X$	$\Delta Y$
0°	208	208
30°	271	208
60°	313	208
88.125°	327	208

and normalized pressures of these levels are given in Table 2.

The scheme of computing radiative heating and cooling is identical with that described by Manabe and Strickler (1964) and Manabe and Wetherald (1967). The scheme consists of two parts—solar radiation and longwave radiation. For this study, the solar insolation of January is assumed. The diurnal variation of solar radiation is not taken into account for the sake of simplicity. The climatological distribution of water vapor, carbon dioxide, ozone and cloud cover in January are used for this computation. They are specified as a function of latitude and height. The temperatures of the continental surfaces are determined by the requirement of heat balance among the turbulent fluxes of sensible and latent heat and the net fluxes of solar and terrestrial radiation. For the sake of simplicity, the ground surface is assumed to have no heat capacity. On the other hand, it is assumed that the sea surface has an infinite heat capacity. The normal distribution of sea surface temperature in February, which has been compiled by the Hydrographic Office (1944) and shown in Fig. 2.2 is used as a lower boundary condition. Before the numerical integrations were completed, it was found that the Hydrographic Office (1964) had published an improved version of the sea surface temperature distribution which is quite different from the

TABLE 2. The approximate heights and the normalized pressure of vertical finite-difference levels of the models.

Level	Normalized pressure $p/p_{surf}$	Height (m)
0.5	0.00000000	$\infty$
1.0	0.01594441	27,900
1.5	0.04334139	21,370
2.0	0.07000000	18,330
2.5	0.11305591	15,290
3.0	0.16500000	12,890
3.5	0.24081005	10,500
4.0	0.31500000	8,680
4.5	0.41204675	6,860
5.0	0.50000000	5,430
5.5	0.60672726	4,010
6.0	0.68500000	3,060
6.5	0.77337055	2,110
7.0	0.83500000	1,490
7.5	0.90154066	860
8.0	0.94000000	520
8.5	0.98010000	170
9.0	0.99000000	80
9.5	1.00000000	0

old version. Nevertheless, the old version was used for the sake of the coherence of the numerical experiments.

The prognostic system of water vapor consists of contributions by the three-dimensional advection of water vapor, evaporation from the earth's surface, so-called "moist convective adjustment," and condensation. This prognostic system is described in detail by Manabe *et al.* (1965). The schemes for computing the hydrology of the ground surface are very similar to those described by Manabe (1969). The rates of change of soil moisture and snow depth are computed based upon the budget of water, snow and heat. It is important to note that snow cover has a very large effect upon the heat balance of the earth's surface by markedly increasing the albedo of the ground surface.

### b. Time integration

As explained in the Introduction, the numerical time integrations are performed with and without the effects of mountains. For the ease of identification, the model with mountains is called the M-model and that with no mountains is called the NM-model.

The initial condition for the numerical time integration of the M-model is a zonal mean state which was obtained from the integration of the hemispheric model (Manabe *et al.*, 1965). First, the global model is integrated using a coarse computational resolution (grid size of about 500 km) for a period of 302 days. Then, the time integration is continued for a period of 70 days after halving the grid size from about 500 km to 250 km. The time mean state which is discussed in the following section is obtained by averaging over the period of the last 40 days of each model. The averaging period of 40 days was chosen because it is long enough to eliminate most of the transient components of the disturbances in the model atmosphere. For further discussion of this subject, see Appendix A.

The initial condition for the time integration of the NM-model is similar to the state on the 60th day of the integration of the high-resolution M-model. In order to minimize the shock caused by the removal of the mountains, it is assumed that the initial distribution of sea level pressure is constant everywhere rather than using the distribution of surface pressure of the M-model. The NM-model was integrated for a period of 62 days. The time mean state of the NM-model described in the following section is obtained by averaging over the last 40-day period of this integration.

Fig. 2.3 shows how the global mass integral of eddy kinetic energy of the high-resolution model changes with time. This result indicates that eddy kinetic energy in the M-model fluctuates around an average value of  $70 \text{ J cm}^{-2}$  and does not seem to have a linear trend. On the other hand, eddy kinetic energy in the NM-atmosphere has not attained a similar quasi-steady state toward the end of the integration. Therefore, it is desirable to extend the time integration of the NM-

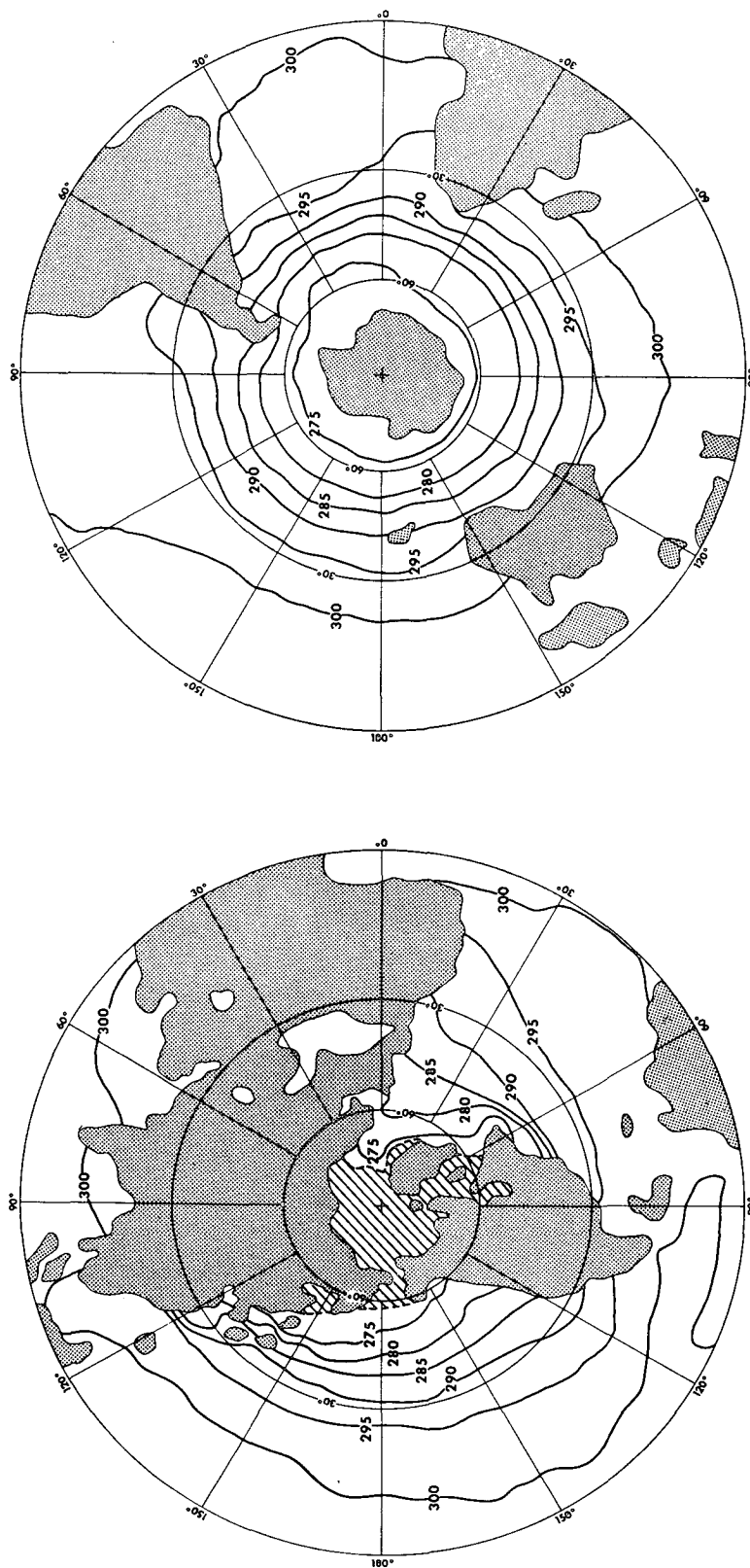


FIG. 2.2. Polar stereographic maps of the distribution of sea surface temperature ( $^{\circ}\text{K}$ ) adopted for the model. The areas covered by thick sea ice are hatched.

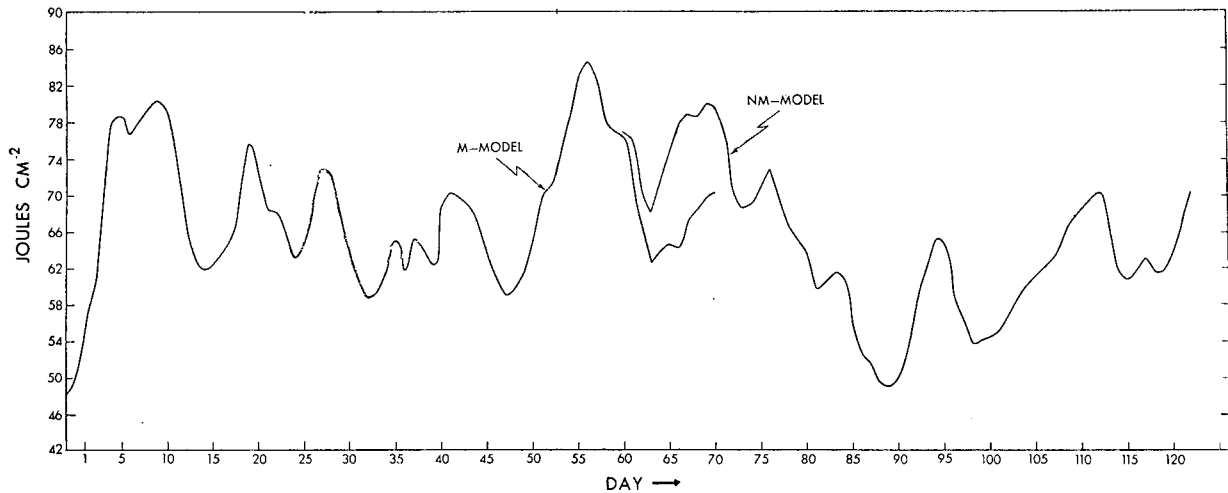


FIG. 2.3. Daily history of the global integral of eddy kinetic energy for the M- and NM-models. The day count starts from the beginning of the integration of the high-resolution version of the M-model.

model further in order to obtain stable statistics describing the state of the NM-atmosphere. Nevertheless, the numerical integration was not extended beyond the 62-day period due to the limitation of computer time.

### 3. Zonal mean state

#### a. Zonal wind

The latitude-height distributions of the time mean zonal wind for both the M- and NM-models are shown in Fig. 3.1. According to this figure, the intensity of the zonal wind in the troposphere is affected little by mountains, whereas the zonal wind in the stratosphere of the NM-model is significantly stronger than that of the M-model. One can compare the distributions of zonal wind in the model atmospheres with the actual distribution of zonal wind (Newell *et al.*, 1971) shown at the top of Fig. 3.1. According to this comparison, the intensity and the distribution of the zonal wind are realistic in the model tropospheres. On the other hand, they are quite different from reality in the model stratospheres. For example, the jet stream in the winter (northern) stratosphere of the M-model is too strong by a factor of more than 2 and is located too far south. The main cause for these discrepancies has not been identified. In the summer (southern) stratosphere of the M-model, weak westerly flow is evident in the middle latitudes. It was found that this unrealistic feature can be improved by incorporating the effects of seasonal variation in the model (see Manabe and Hahn, 1974).

#### b. Zonal mean temperature

In Fig. 3.2 the latitude-height distribution of zonal mean temperature in the M-model is compared with the observed distribution compiled by Newell *et al.* In

general, the agreement between the two distributions is good. However, the temperature of the model stratosphere is too low by about 30K in the arctic region. According to the thermal wind relationship, this unrealistically low temperature is consistent with the excessive stratospheric zonal wind in the model stratosphere which is described in the preceding subsection. For further discussion of the thermal structure of the model atmosphere, see Holloway and Manabe (1971). Since the difference between the thermal structure of the M-model and that of the NM-model is not very pronounced, it is not discussed here.

#### c. Sea level pressure

In Fig. 3.3 the latitudinal distribution of the zonal mean sea level pressure in both model atmospheres is compared with the distribution in the actual atmosphere. This comparison reveals that both models yield too high a pressure at the arctic and too low a pressure around 60N. According to Holloway and Manabe, the excessively high pressure at the arctic of the model resulted from the systematic bias of the truncation error involved in the finite-difference computation with the irregular grid system adopted for this study. Holloway *et al.* (1973) demonstrated that this bias can be removed by adopting the so-called latitude-longitude grid system in which grid points are lined up along latitude circles and meridians.

The sea level pressure is also too high at the antarctic of the model. Unfortunately, Holloway *et al.* found that the change of the grid system is not effective in eliminating this unrealistic feature. As discussed in Appendix B, the finite-difference representation of the pressure gradient force has a systematic error, particularly in the area of steep mountain ranges, and does not satisfy the integral constraint of momentum which the continuous representation requires. Although it is not

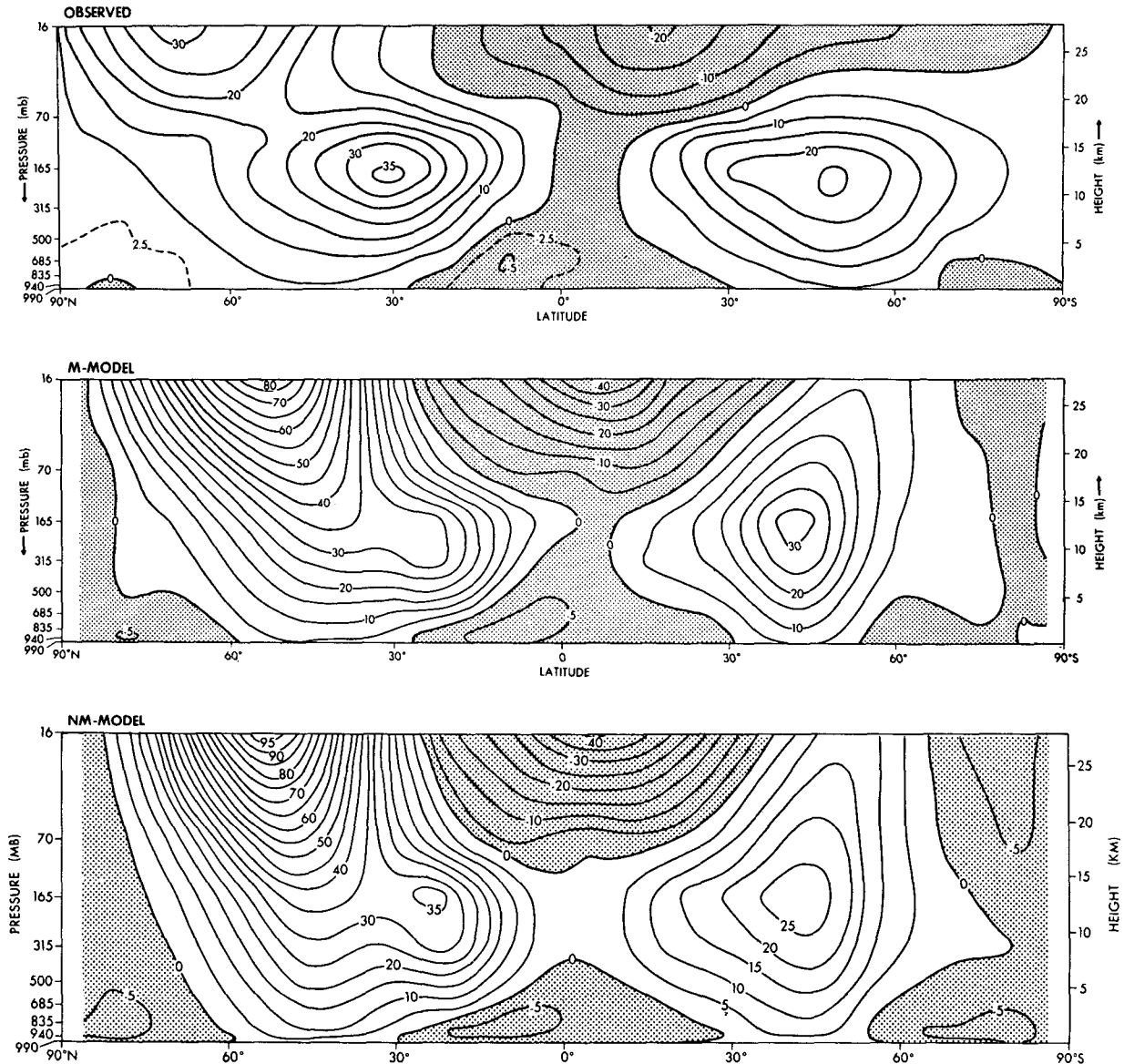


FIG. 3.1. The latitude-height distribution of the time mean zonal wind ( $\text{m sec}^{-1}$ ): top, observed (Newell *et al.*, 1971); middle, the M-model; bottom, the NM-model.

certain whether this inconsistency is responsible for the discrepancy mentioned above, further reduction of truncation errors in the computation of the pressure gradient force and vertical  $p$ -velocity seems to be required for the successful simulation of sea level pressure.

In lower latitudes of both models, the distribution of zonal mean sea level pressure is very realistic. The model simulates successfully the low pressure belt at the equator and the high pressure belt in the subtropics.

#### d. Eddy kinetic energy

Before discussing the effects of topography upon the kinetic energy of stationary disturbances, it is necessary

to define the eddy kinetic energy of stationary and transient disturbances. The kinetic energy of stationary eddies  $K_E^{ST}$  is defined by

$$K_E^{ST} = \frac{1}{2} [(\overline{u})^{*2} + (\overline{v})^{*2}], \quad (3.1)$$

and that of transient eddies  $K_E^{TR}$  is defined by

$$K_E^{TR} = \frac{1}{2} [(\overline{u}')^{*2} + (\overline{v}')^{*2}], \quad (3.2)$$

where  $u$  and  $v$  denote the zonal and meridional component of wind,  $[ ]$  and  $( )$  indicate the zonal and time-mean operators, and  $( )^*$  and  $( )'$  denote the deviations from zonal and time-mean, respectively. The total

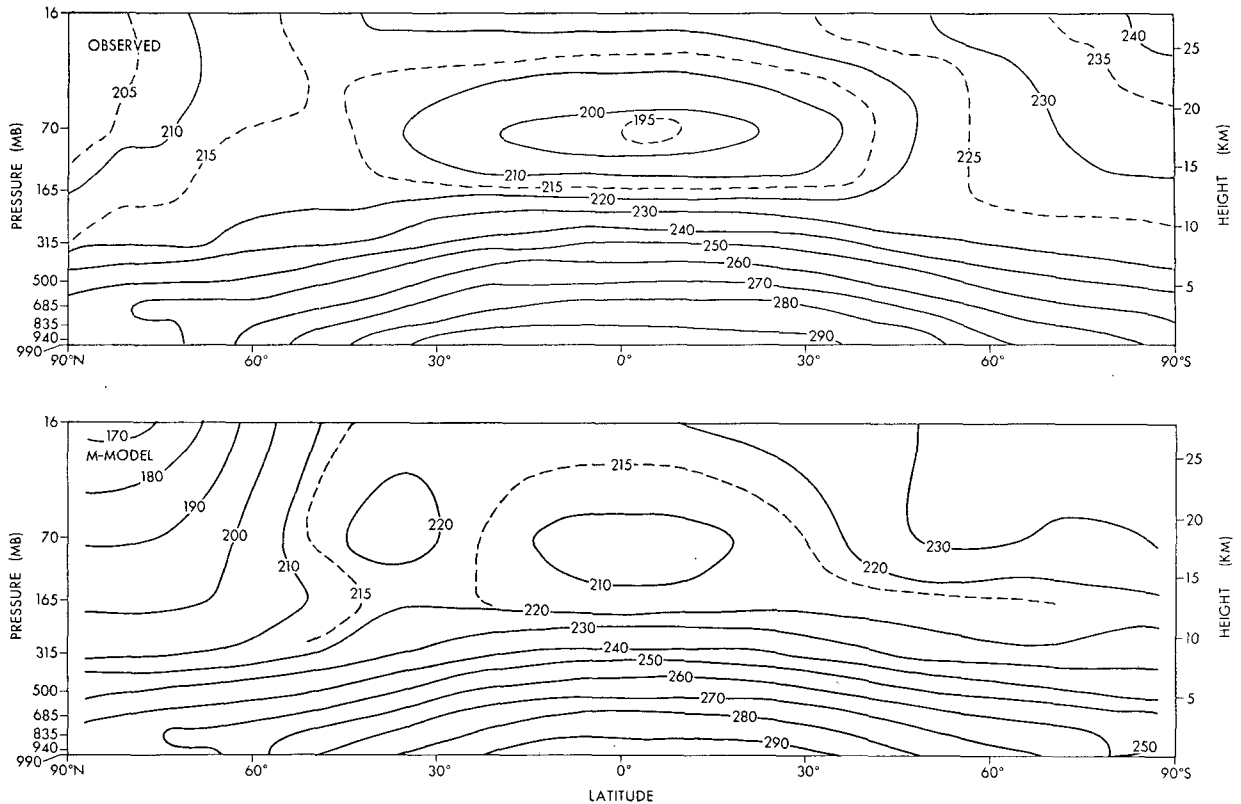


FIG. 3.2. Latitude-height distribution of zonal mean temperature ( $^{\circ}\text{K}$ ): top, observed (Newell *et al.*, 1971); bottom, M-model.

kinetic energy  $K_E$  which is the sum of  $K_E^{ST}$  and  $K_E^{TR}$  is given by

$$K_E = K_E^{ST} + K_E^{TR} = \frac{1}{2} [\overline{u'^2} + \overline{v'^2}]. \quad (3.3)$$

The tropospheric integrals of  $K_E$ ,  $K_E^{ST}$  and  $K_E^{TR}$  in

both model atmospheres are shown as a function of latitude in Fig. 3.4. Comparing the distributions of the stationary and transient components of eddy kinetic energy of the M-model with those of the NM-model, one finds that mountains are responsible for increasing the kinetic energy of stationary disturbances but decreasing

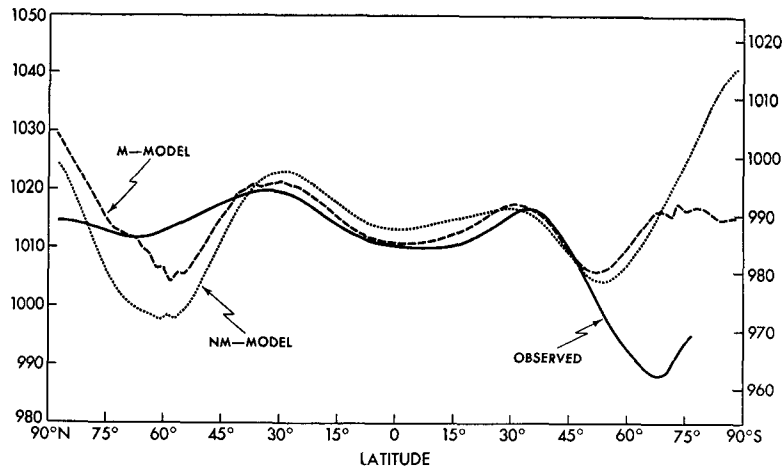


FIG. 3.3. Latitudinal distribution of zonal mean sea level pressure (mb)—observed (Mintz, 1965), solid line; M-model, dashed line; NM-model, dotted line: left-hand side, vertical scale for observed and M-model; right-hand side, vertical scale for NM-model.



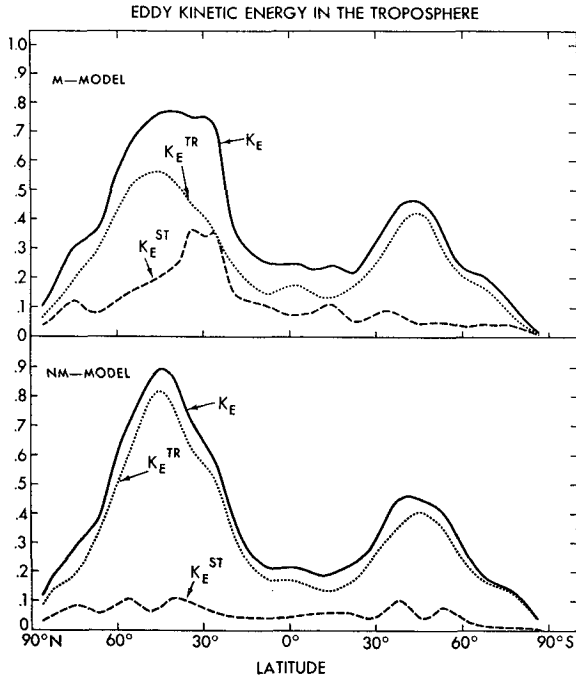


FIG. 3.4. The latitudinal distribution of  $K_E$  (solid line),  $K_E^{ST}$  (dashed line) and  $K_E^{TR}$  (dotted line) integrated over the model troposphere in units of  $100 \text{ J cm}^{-2}$ . The troposphere is defined as the part of the model atmosphere below 240 mb. Top, the M-model; bottom, the NM-model.

that of transient disturbances. The total eddy kinetic energy, which is the sum of the two components of eddy kinetic energy, is altered little by the mountains. Fig. 3.5 shows the ratio of the tropospheric vertical mass integral of stationary eddy kinetic energy to that of total eddy kinetic energy for both models. According to this figure, the relative magnitude of the stationary component is particularly large in the Northern Hemisphere and the Antarctic continent where major mountain ranges are located.

In Fig. 3.6 we show the latitudinal distributions of the tropospheric vertical integrals of  $K_E$ ,  $K_E^{ST}$  and  $K_E^{TR}$ , as computed by Oort and Rasmusson (1971) for the actual atmosphere. Unfortunately, the equation used by Oort and Rasmusson in defining the kinetic energy of

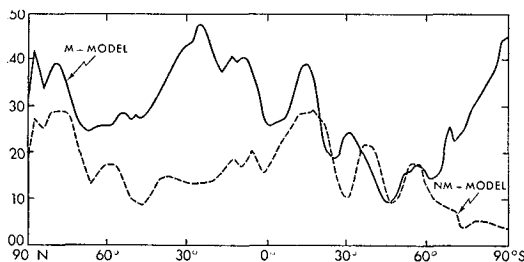


FIG. 3.5. The latitudinal distribution of the ratio of  $K_E^{ST}$  to  $K_E^{TR}$ : M-model, solid line; NM-model, dashed line. (Here,  $K_E^{ST}$  and  $K_E^{TR}$  represent the mass integrals over the model tropospheres).

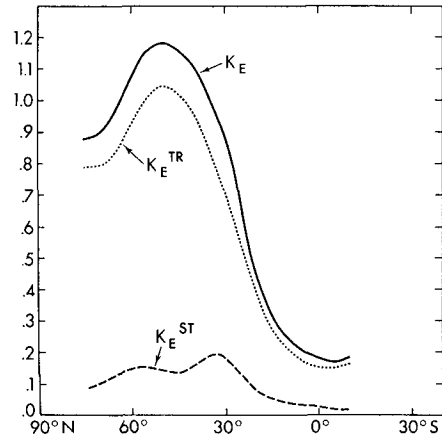


FIG. 3.6. The observed latitudinal distribution of  $K_E$ ,  $K_E^{ST}$  and  $K_E^{TR}$  integrated over the troposphere in units of  $100 \text{ J cm}^{-2}$ . The troposphere is defined as the part of the atmosphere below the 250-mb level. (After Oort and Rasmusson, 1971.)

transient eddies is slightly different from (3.2),<sup>1</sup> and another difference lies in the period over which the time mean operator is applied.<sup>2</sup> For example, his transient component in January represents the deviation from the average value over five Januaries of five consecutive years, whereas in this study it represents the deviation from the average over the last 40-day period of each time integration. Nevertheless, these distributions are compared with the eddy kinetic energy in the M-model atmosphere. According to this comparison, the kinetic energy of stationary disturbances in the Northern Hemisphere of the M-model is significantly larger than that in the actual atmosphere. On the other hand, the kinetic energy of transient disturbances in the M-model atmosphere is too small as compared with that in the actual atmosphere. According to crude estimates, these differences partly resulted from the differences in the definition of eddy kinetic energies mentioned above. However, there may be other reasons for these discrepancies. Recent results of Manabe *et al.* (1970b) indicate that the increase of the finite-difference resolution not only increases the accuracy of finite-difference computation but also decreases the scale at which the horizontal subgrid-scale viscosity is most effective.

<sup>1</sup> The eddy kinetic energy of transient eddies, which is adopted by Oort and Rasmusson, is given by

$$K_E^{TR} = \frac{1}{2} [\overline{u'^2} + \overline{v'^2}].$$

It includes the eddy kinetic energy of transient zonal mean flow, i.e.,

$$\frac{1}{2} (\overline{[u']^2} + \overline{[v']^2}).$$

In the model atmosphere, the magnitude of this term is about 10–15% of  $K_E^{TR}$ .

<sup>2</sup> According to Oort (private communication), the  $K_E^{TR}$  defined for one January is about 20% smaller than that defined for five Januaries. Naturally,  $K_E^{ST}$  is also affected by the length of the analysis period in an opposite way such that the sum of these two energies is unaltered.

This allows more transient disturbances to develop in the model atmosphere. Therefore, it is probable that further increase of the computational resolution would yield more realistic values of the kinetic energy of transient eddies.

The latitude-height distributions of eddy kinetic energy in both the M- and NM-atmospheres are shown in Fig. 3.7. A marked increase in the kinetic energy of the stationary disturbances due to the effects of mountains is evident in the Northern Hemisphere of the M-model, particularly in the stratosphere. As pointed out already, the kinetic energy of transient eddies in the model troposphere decreases as a result of incorporating mountains into the model. However, it is not so in the model stratosphere, where the kinetic energy of transient as well as stationary eddies increases due to the effects of mountains.

#### 4. The structure of stationary disturbances

##### a. Northern Hemisphere

The general features of the stationary disturbances in the Northern Hemisphere of the model atmosphere are evident in Fig. 4.1a, which shows the time-mean maps of the heights of isobaric surfaces in both the M- and the NM-model atmospheres as well as those in the actual atmosphere (Taljaad *et al.*, 1969).<sup>3</sup> In general, the geopotential height contours of isobaric surfaces are more axial-symmetric with increasing altitude partly due to the increase of zonal currents with height. In the M-model such a trend is less obvious because of the predominance of stationary disturbances in the upper troposphere due to the effects of mountains. In this subsection the relative importance of heating and topography is discussed by comparing the features of stationary disturbances at various isobaric levels of both the M- and NM-models.

##### 1) 1000-MB LEVEL

At the 1000-mb level of the M-model, the Aleutian low, Icelandic low and Siberian high are identifiable in qualitative agreement with the features of the observed distributions. However, the Aleutian low is so intense and excessive that it invades the western half of the

North American continent where surface pressure is relatively high in the actual atmosphere. Since the Aleutian low predominates in the NM-model as well as in the M-model, one can infer that mountains are not necessary for the formation of the low. Instead, the temperature contrast between land and sea seems to be responsible for the maintenance of the Aleutian low. [Recently, Manabe (1969) obtained a similar conclusion based upon the results from a mountainless model with highly idealized geography.] The present result is quite different from the result of Kasahara and Washington (1969), who emphasized the importance of mountains for the maintenance of the Aleutian low. The cause for the difference between their result and ours is not clear. It should be pointed out, however, that the Aleutian low in their M-model is unrealistically weak.

Orography seems to play a very significant role in the maintenance of the so-called "Siberian high" in the model atmosphere. In the NM-model, this anticyclone is located at about 30N over the Eurasian continent; whereas, in the M-model, it is located at about 45N, i.e., slightly to the south of the observed location of the Siberian high. Another notable difference between the two models is that the high is more intense in the M-model than in the NM-model. In short, present results suggest that mountains are responsible for the intensification and the northward shift of the anticyclone over the Eurasian continent. Based upon the results from his numerical experiments, Mintz (1965) emphasized the importance of mountains on the formation of the Siberian high. He pointed out that the high does not appear when the Himalayan mountain chain is removed in his model. Since his report does not include the sea level pressure of his NM-model, it is not possible to determine whether his results are similar to present results. The numerical experiments of Kasahara and Washington (1968) also suggest that orography is responsible for intensifying the anticyclone over the Eurasian continent in agreement with the results of this study. However, the northward shift of the anticyclone mentioned above is not evident in their results. Accordingly, the anticyclone in their M-model is located at 35N, i.e., at too low a latitude. Despite the differences among various numerical experiments, it seems to be highly probable that the Tibetan Plateau is responsible for intensifying the anticyclone over the Eurasian continent during winter.

In high latitudes, the geopotential height of the 1000-mb level is much higher than the observed. As pointed out already, this discrepancy is mainly due to the systematic bias of the model. (See the first paragraph of Section 3c for further discussion of this subject.)

In their study of the effects of heat sources upon the field of stationary flow in the atmosphere, Smagorinsky

<sup>3</sup> The geopotential heights of an isobaric surface of the M-model are systematically higher than those of the NM-model. This difference results from the difference in sea level pressure between the two models. Although the total air masses of the two models are identical with each other, the mean sea level pressure of the M-model is 1014 mb and is about 26 mb higher than that of the NM-model due to the mountain topography. Therefore, the height of the  $p$  mb level of the M-model corresponds approximately to that of the  $p \times (988/1014)$  mb level of the NM-model. In order to compare the maps of geopotential heights of the two models, it is desirable to add 205, 204, 203, 205, 210 and 263 m to the geopotential heights of the 1000-, 850-, 700-, 500-, 300- and 30-mb levels of the NM-model, respectively.

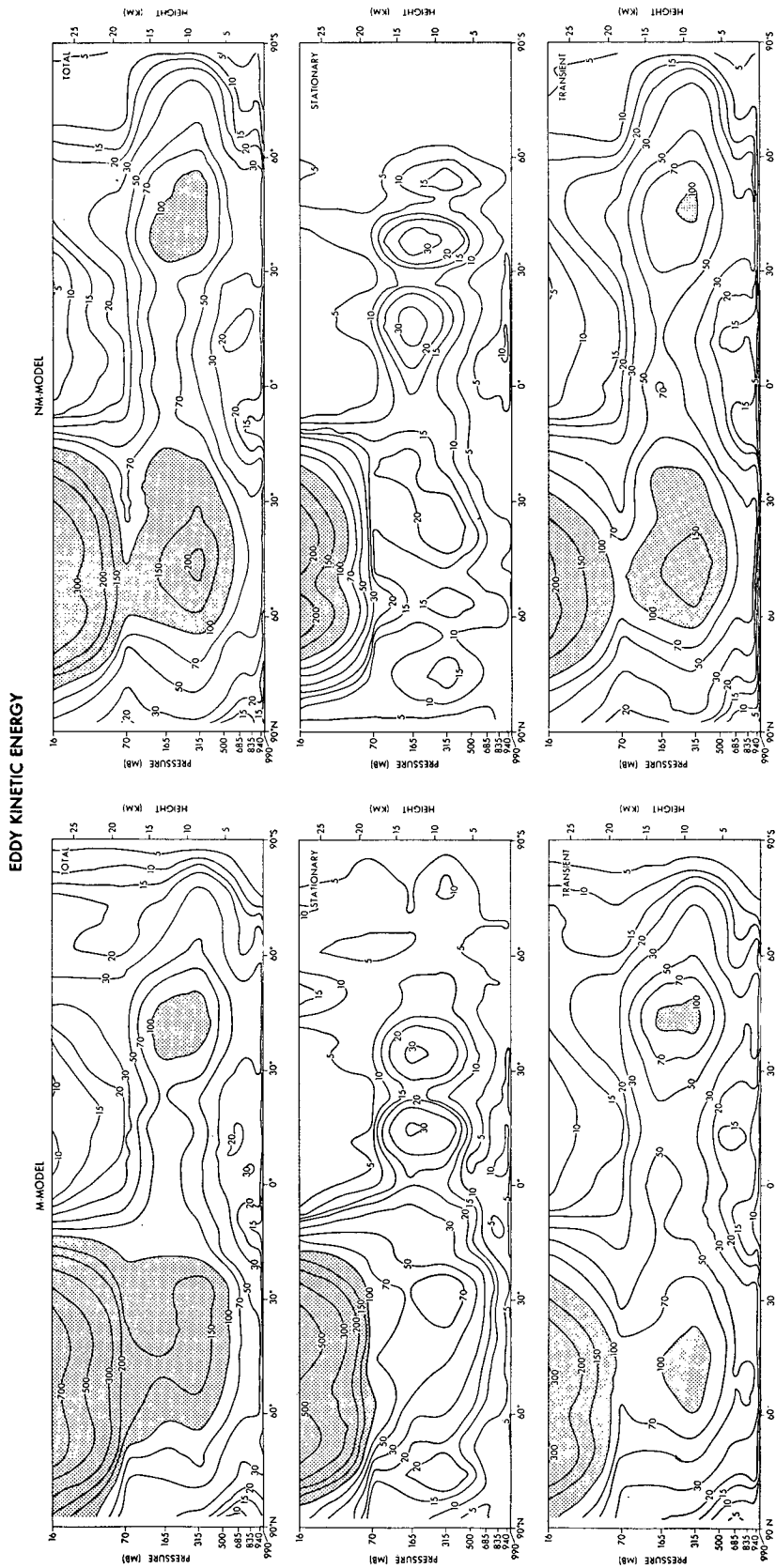


FIG. 3.7. The latitude-height distribution of  $K_E$ ,  $K_E^{ST}$  and  $K_E^{TR}$  (top, middle, bottom) for the M-model (left) and the N-M-model (right); units,  $10^{-3} \text{ J cm}^{-2} \text{ mb}^{-1}$ .

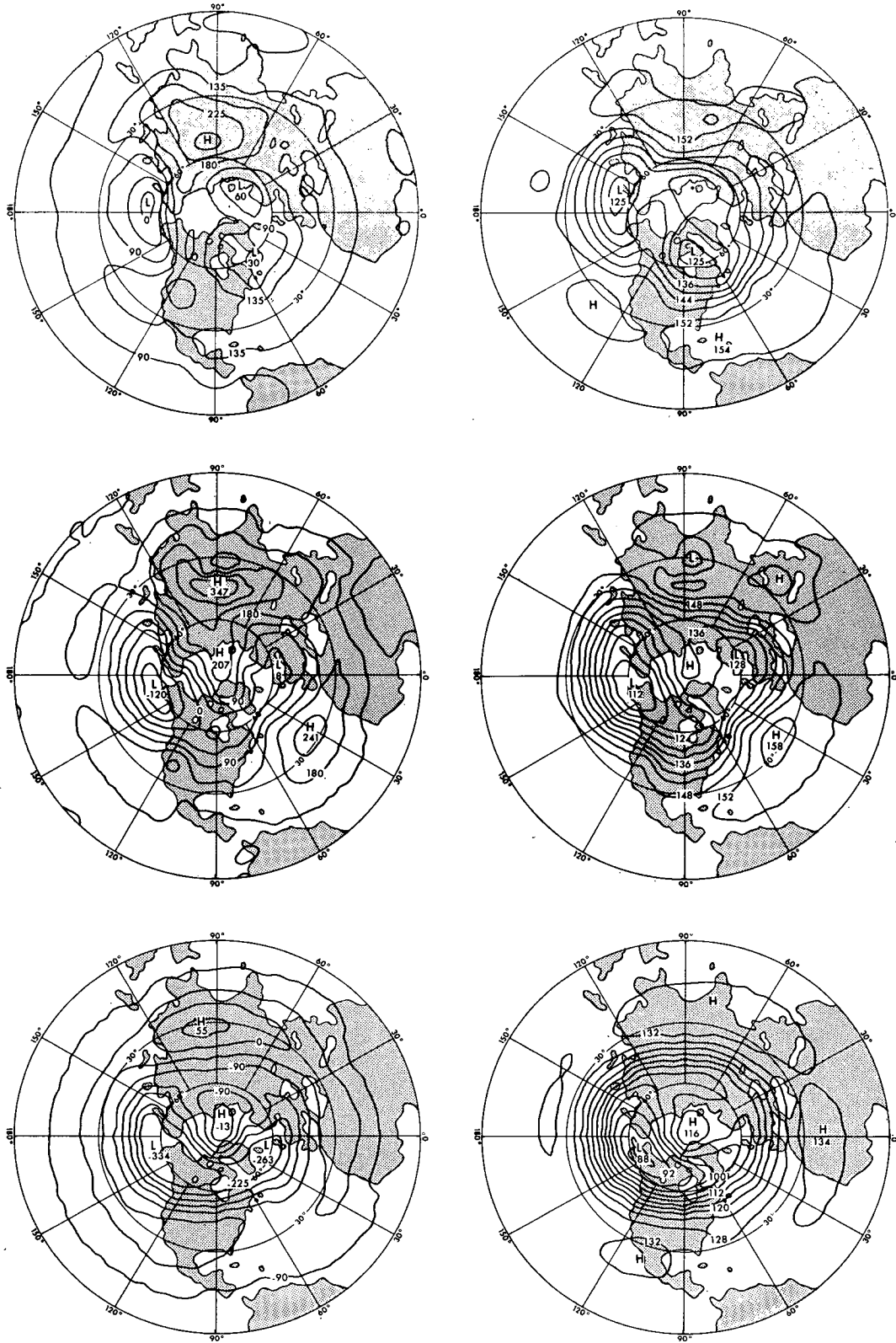


FIG. 4.1a. Time-mean geopotential height maps of the Northern Hemisphere at 1000 mb (left) and 850 mb (right). Units for 1000-mb case, geopotential meters; and for 850 mb case, geopotential decameters. Top: observed [Oort and Rasmusson (private communication): average over five Januaries, 1959-63]; middle: the M-model; bottom: the NM-model.

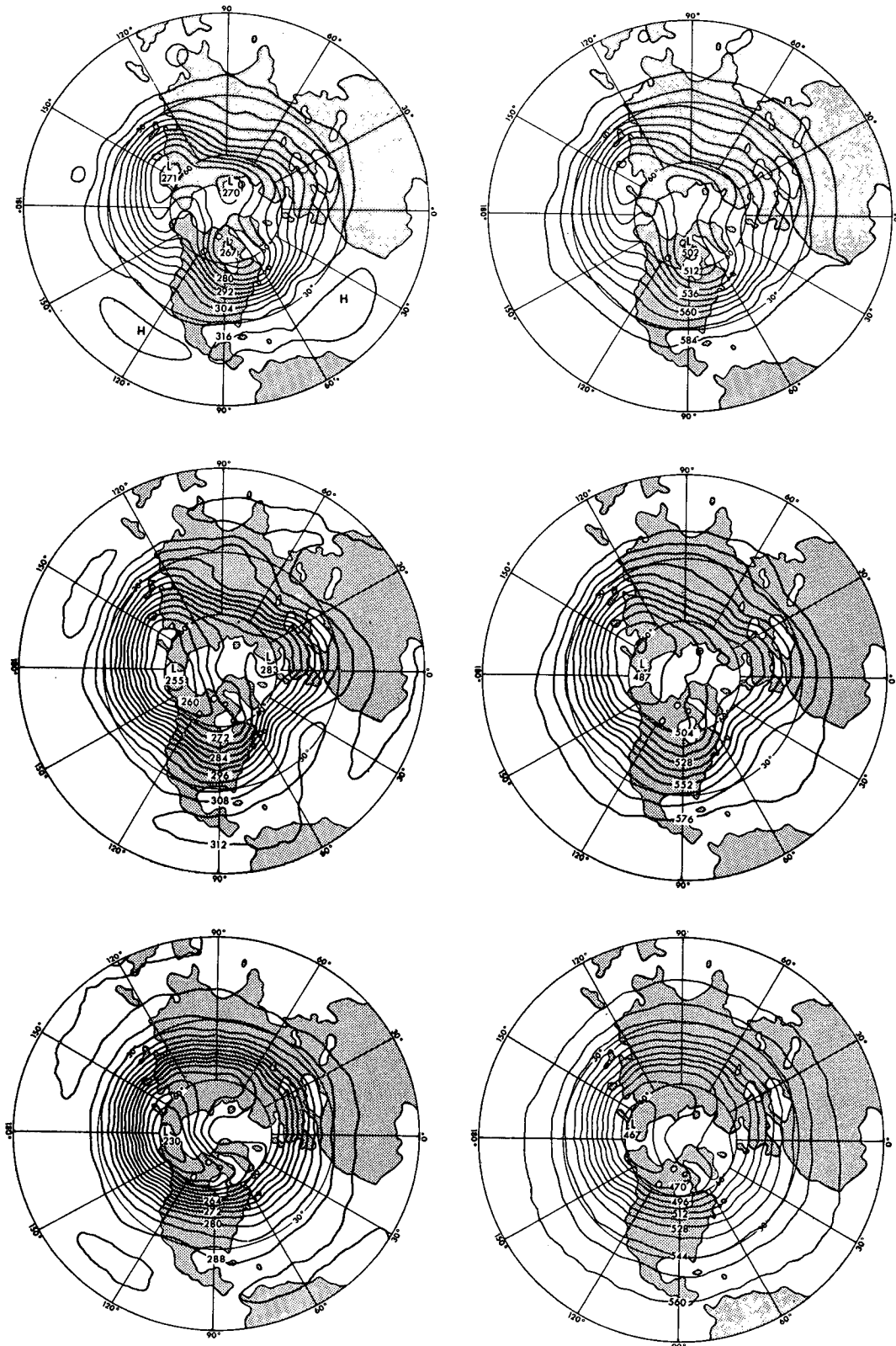


FIG. 4.1b. As in Fig. 4.1a except for 700 mb (left) and 500 mb (right): units, geopotential decameters.

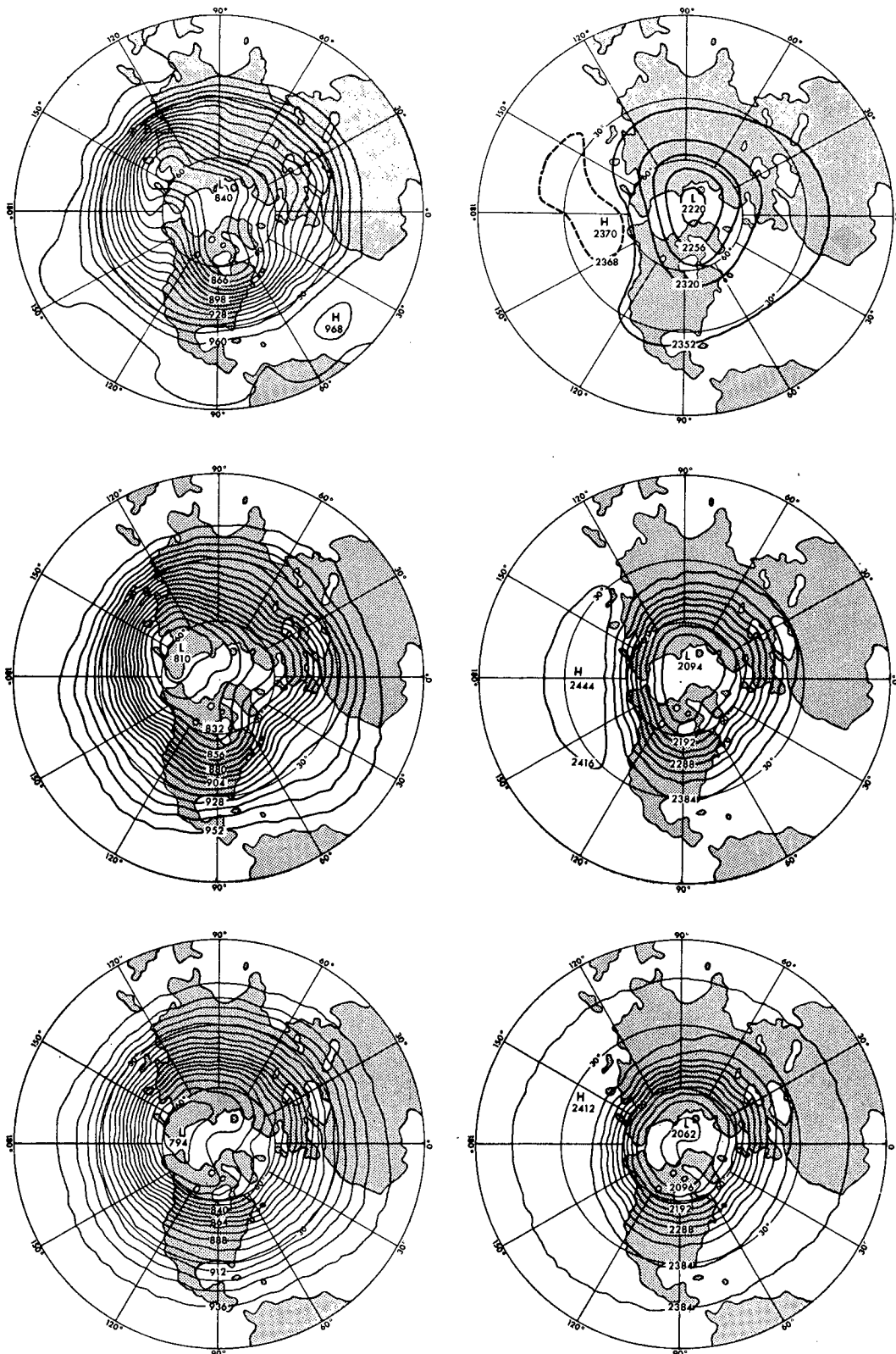


FIG. 4.1c. As in Fig. 4.1a except for 300 mb (left) and 30 mb (right): units, geopotential decameters.

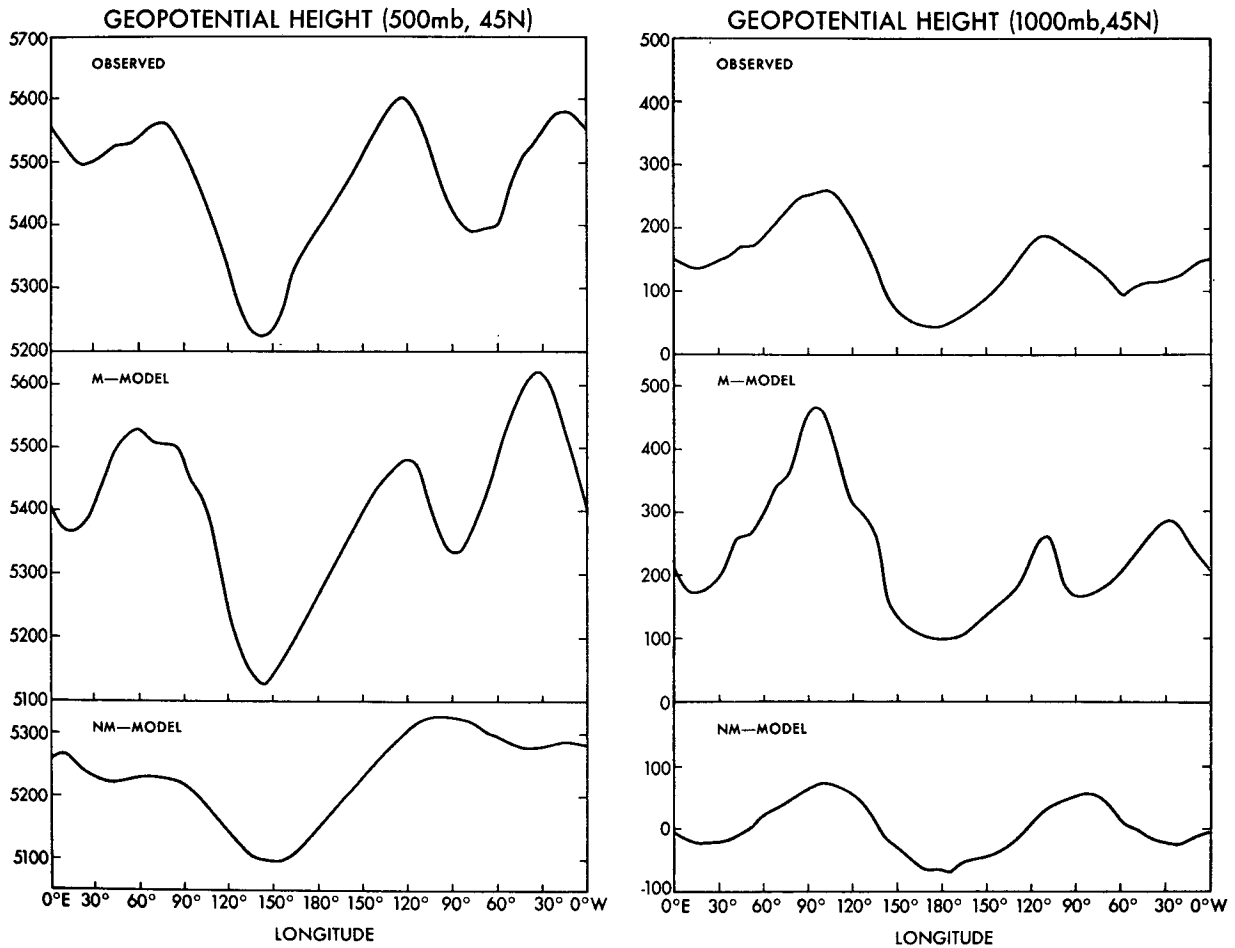


FIG. 4.2. Longitudinal variation of the time-mean geopotential height (geopotential meters) of 500- and 1000-mb levels at 45N: top, observed (Ort and Rasmusson, private communication); middle, the M-model; bottom, the NM-model.

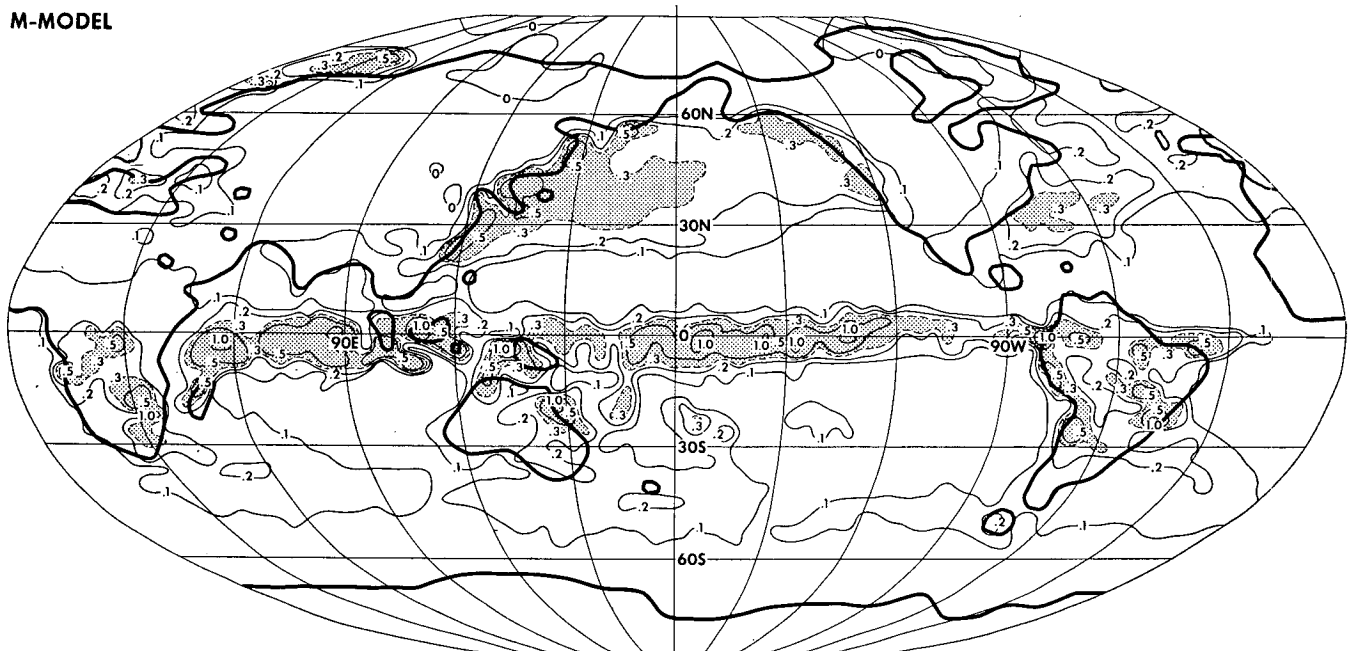
(1953) and Döös (1962) show that the trough of sea level pressure is located about 20° longitude to the east of the area of the maximum heat source. In the right-hand side of Fig. 4.2, the longitudinal distributions of the time-mean geopotential height of the 1000-mb level at 45N of both the M- and NM-models are shown together with that of the actual atmosphere. Also, the horizontal distribution of the rate of heating for both model atmospheres is shown in Fig. 4.3 (here, the rate of heating is the sum of the contributions from condensation and the upward flux of sensible heat from the earth's surface.) Examining Figs. 4.2 and 4.3, one finds that the belt of lower pressure is located to the east of the area of maximum heating in qualitative agreement with the results from the studies of Smagorinsky and Döös. In the NM-model, both the Aleutian and Icelandic lows are located about 30° east of the areas of relatively large heating rate which appear over the northwestern part of the Pacific and the Atlantic, respectively. In the M-model, the intense Aleutian low is also located to the east of the area of intense heating. However, the maximum heating off the east coast of

North America is much weaker than the estimate of the heating based upon Budyko's study (1963). Therefore, it is understandable that the Icelandic low is too weak as compared with the actual one (see Fig. 4.1a). In general, the correspondence between the heat sources and low pressure is poorer in the M-model than in the NM-model, probably due to the effects of mountains.

## 2) 500-MB LEVEL

The time-mean maps of the geopotential heights of the 500-mb level in the model atmospheres and the actual atmosphere are contained in Fig. 4.1b. This figure indicates that a well-developed Aleutian low predominates in both the M- and NM-atmospheres. It is very intense and extends to Alaska where the ridge of pressure is located in the actual atmosphere. Accordingly, the agreement between the distributions of geopotential height of the 500-mb level surface in the M-model atmosphere and that in the actual atmosphere is particularly poor in higher latitudes. However, the distributions in the middle and low latitudes of the

## M-MODEL



## NM-MODEL

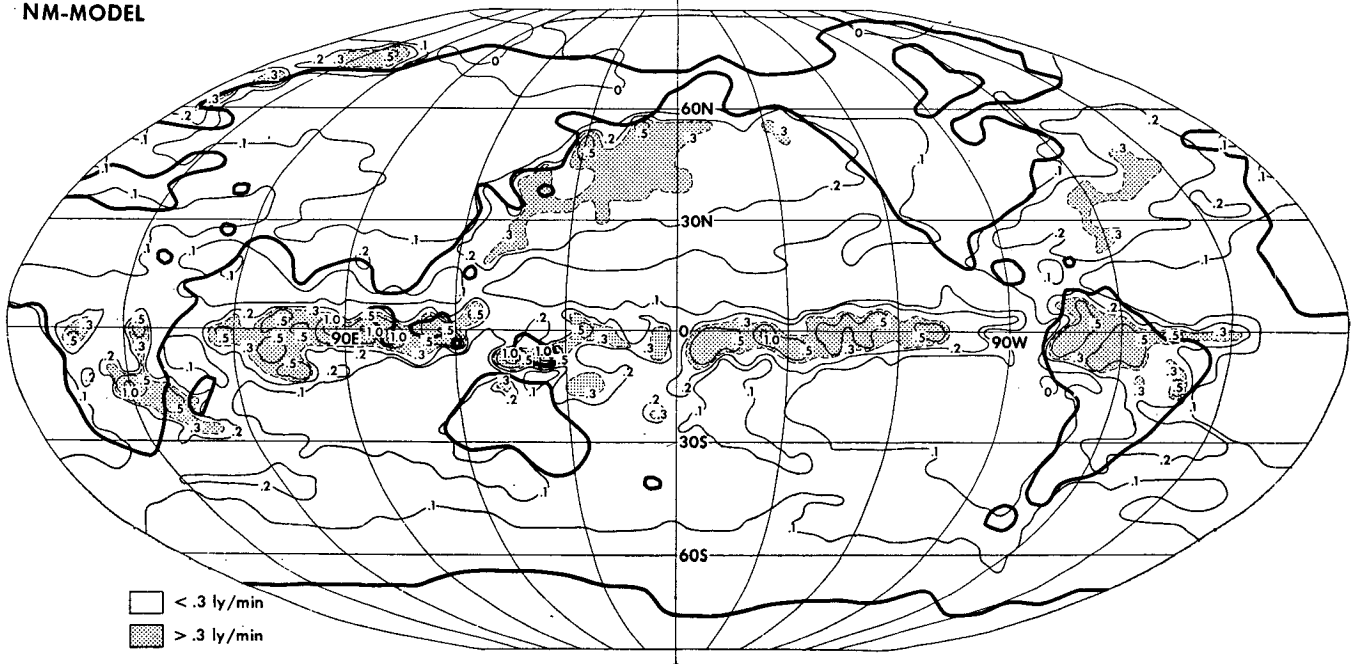
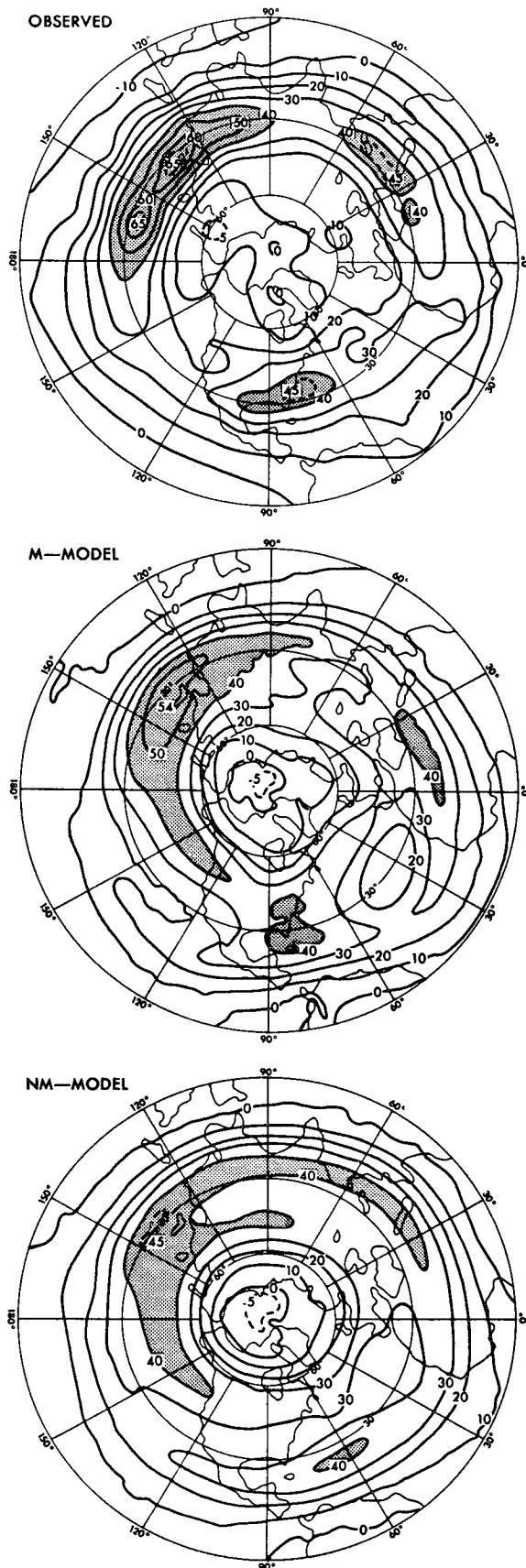


FIG. 4.3. Horizontal distribution of the rate of heating ( $\text{ly min}^{-1}$ ) due to condensation, moist convection and sensible heat flux: upper half, the M-model; lower half, the NM-model.

M-model are much more realistic than those in higher latitudes. For example, well-developed troughs in the lee of the Tibetan Plateau and the Rocky Mountains are simulated successfully by the M-model. For further examination of the geopotential heights in the middle latitudes of the models, reference should be made to Fig. 4.2. In the left-hand part of this figure, the longitudinal distribution of the time-mean geopotential

heights of the 500-mb surface along the 45N latitude circle in both models is compared with that in the actual atmosphere. According to this comparison, the longitudes of the troughs and ridges at 500 mb in the M-atmosphere agree with those in the actual atmosphere much better than those in the NM-atmosphere. Also, Fig. 4.2 shows that the amplitude of the longitudinal variation of the geopotential height in the





former is much larger than the latter, which indicates the relative importance of mountains in maintaining the stationary disturbances around the 500-mb level.

### 3) UPPER TROPOSPHERE

Fig. 4.1c indicates that, in the M-model atmosphere, the general features of the distribution of geopotential height of the 300-mb level coincide very well with those of the 500-mb level except that the former have a larger meridional gradient than the latter. For example, troughs form in the lee of major mountain ranges such as the Tibetan Plateau and the Rocky Mountains. They tilt from southwest to northeast indicating the poleward transport of angular momentum by stationary disturbances. The contours of geopotential height are concentrated on the eastern side of the lee trough of the Tibetan Plateau implying the prevalence of the jet stream there. These isobaric surface features in the upper troposphere of the M-model are in excellent qualitative agreement with those in the actual atmosphere.

In order to examine further the distribution of the jet stream in the upper troposphere of the M-model, the map of the isotachs of the time-mean zonal component of flow at the 200-mb level of the M-model is compared with the corresponding maps of the NM-model and the actual atmosphere (Fig. 4.4). The observed distribution is obtained by Oort and Rasmusson<sup>4</sup> and represents the average over five consecutive Januaries. This figure indicates that the intensity of the jet stream on the eastern side of the Tibetan Plateau is intensified significantly by the mountains. Also, the local maximum of zonal flow appears over the southeastern part of the United States, i.e., on the eastern side of the lee trough of the Rocky Mountains, again resulting from incorporation of the effects of mountains. In general, the values of the local maxima of the isotachs in the upper troposphere of the M-model are less than the corresponding values in the actual atmosphere. However, it is encouraging that the distribution of the isotachs in the upper troposphere of the M-model is more realistic than that of the NM-model.

Bolin (1950) discussed the influence of circular mountains on the general character of the westerly flow by obtaining a steady-state solution of a simple barotropic model. His solution shows a trough in the lee of the mountain and an intensified zonal flow on the southeastern side of the lee trough. These results seem to be in excellent qualitative agreement with results from the present study.

As mentioned in the Introduction, Kasahara and Washington (1971) performed numerical experiments

<sup>4</sup> Private communication.

FIG. 4.4. The isotachs of the time mean zonal wind ( $m\ sec^{-1}$ ) at the 200-mb level: top, observed [Oort and Rasmusson (private communication) average over five Januaries, 1959-63]; middle, the M-model; bottom, the NM-model.

which are very similar to those of the present study. However, they did not find a significant difference in the intensity of the jet stream resulting from the incorporation of the effects of mountains. The reasons their results differ from the present experiments is not clear.

#### 4) 30-MB LEVEL

Fig. 4.1c shows that at the 30-mb level of the M-model, the intensity of the time-mean zonal current is too strong by a factor of more than 2. However, the circumpolar vortex has an elongated shape and resembles the vortex prevailing in the actual winter stratosphere. Also, an anticyclone is located over the Aleutian Archipelago in agreement with the features of the actual atmosphere. On the other hand, the distribution in the NM-model stratosphere is less realistic and there is no Aleutian anticyclone. Recently, qualitatively

similar results were obtained by Washington (1973). It should be pointed out, however, that the maps represent the average height distribution over the 40-day period during which the distribution changes markedly (see Appendix A). Therefore, the map does not represent a quasi-stationary state. Nevertheless, the elongation of the polar vortex in the NM-model stratosphere is much less than that in the M-model stratosphere, indicating the importance of mountains in maintaining the stationary eddy disturbances in the stratosphere.

#### 5) VERTICAL STRUCTURE

In order to discuss the vertical structure of the stationary disturbances in the model atmospheres, we present in Fig. 4.5 a comparison of the longitude-height distributions of the time-mean meridional component of the wind along the 45N latitude circle in the model

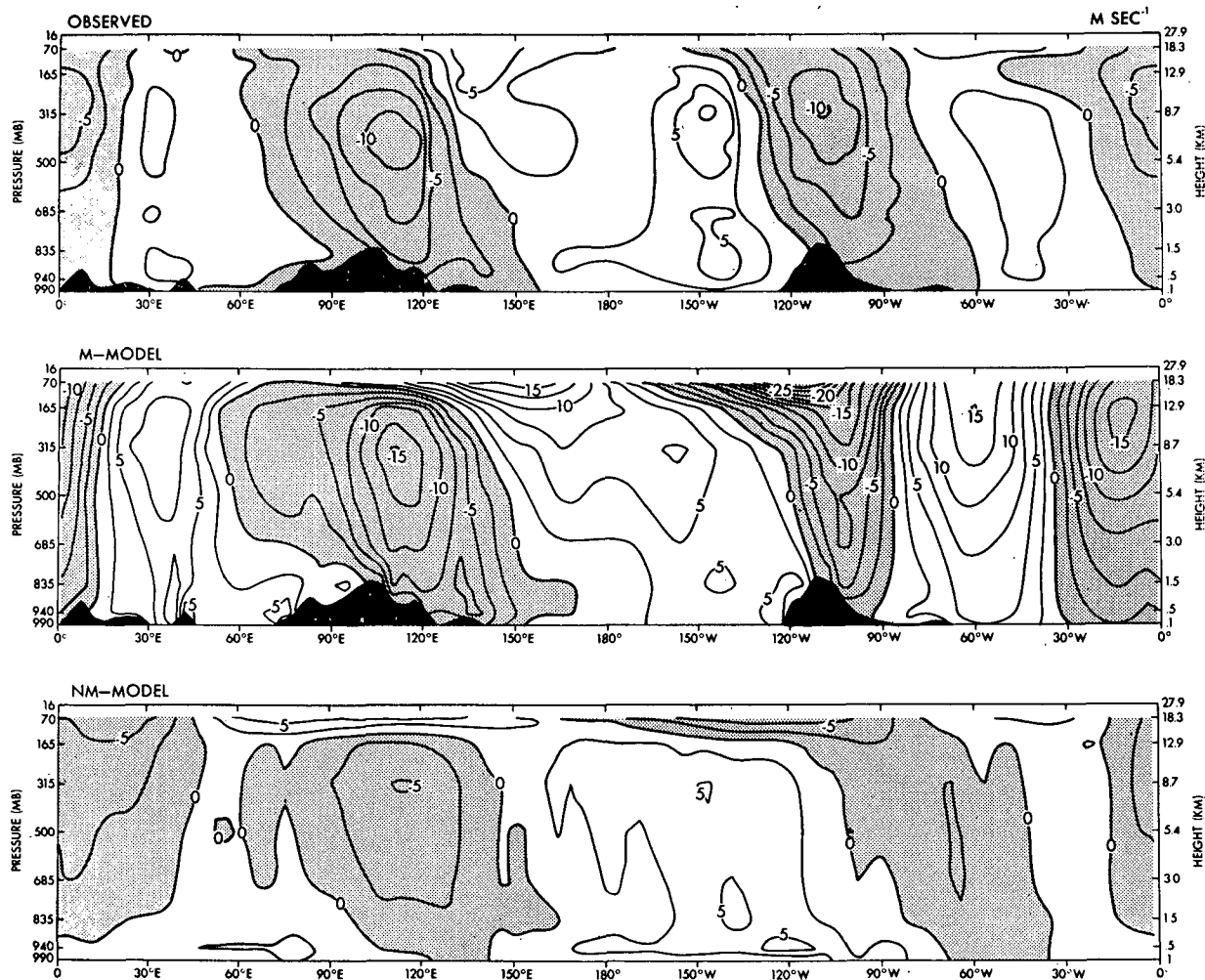


FIG. 4.5. The longitude-height distribution of the time mean meridional component of wind ( $\text{m sec}^{-1}$ ) along the 45N latitude circle: top, observed [Oort and Rasmusson (private communication) average over five Januaries, 1959-63]; middle: the M-model; bottom, the NM-model.

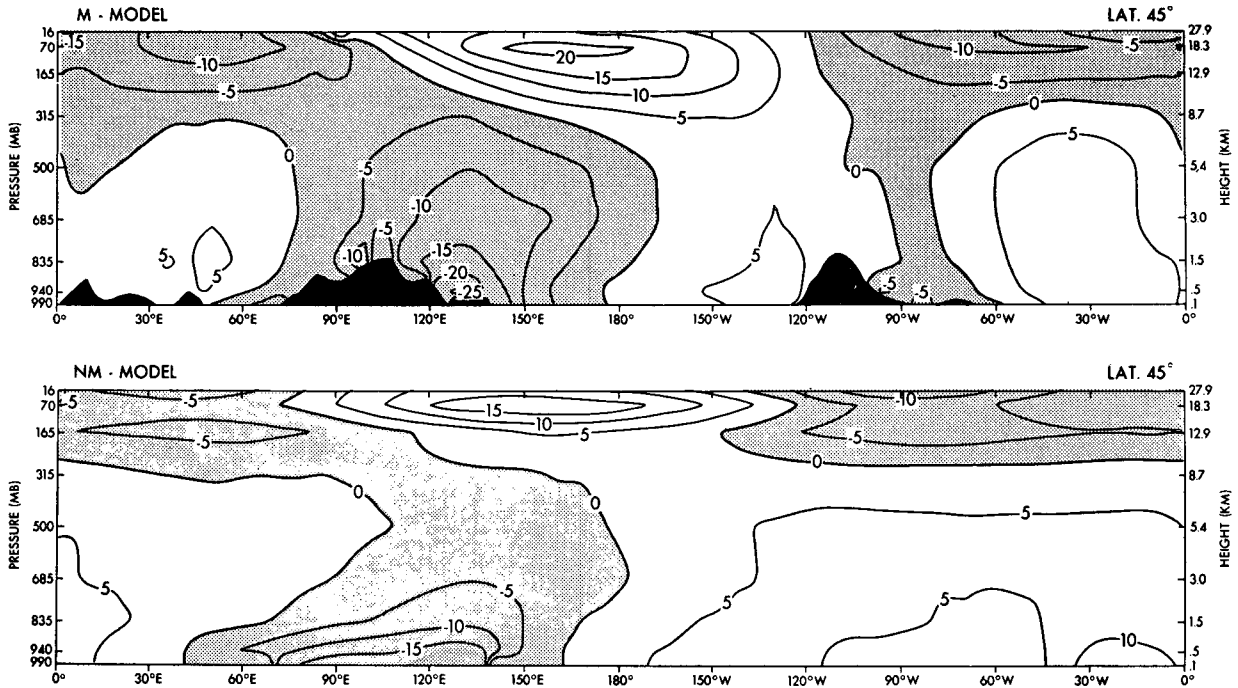


FIG. 4.6. Longitude-height distribution of the deviation of temperature from zonal mean ( $^{\circ}\text{K}$ ): upper half, the M-model; lower half, the NM-model.

atmospheres with the corresponding distribution in the actual atmosphere (Oort and Rasmusson, private communication). We see that the amplitude of the stationary disturbances in the M-model atmosphere is significantly larger than the observed value. Nevertheless, the general features of the distribution of the time-mean meridional component of the wind in the M-model atmosphere agree well with those in the actual atmosphere. On the other hand, the corresponding distribution in the NM-model atmosphere is not realistic. The comparison between the M- and NM-models suggests that mountains affect the distribution of stationary disturbances, particularly in the upper troposphere and the stratosphere of the winter hemisphere.

In the meridional cross sections for the model atmospheres (Fig. 4.5), some of the zero lines tilt westward with increasing height. Smagorinsky (1953) obtained qualitatively similar results in his theoretical study mentioned earlier. Using the so-called thermal wind relationship, one can show that such a tilt implies relatively warm air in front of pressure troughs and relatively cold air in the rear of troughs. The positive correlation between temperature and meridional wind in the M-model atmosphere may be noted by comparing Fig. 4.5 with Fig. 4.6 which shows the longitude-height cross sections of temperature deviation from the zonal mean in both models. Because of the positive correlation, the wave with westward tilt transports heat poleward. In Section 6, it is shown that the stationary eddies in the M-model atmosphere indeed transport heat poleward very efficiently.

#### 6) RECENT THEORETICAL STUDIES

The results so far yield the impression that, during winter, the relative importance of the influence of mountains upon the stationary flow field increases with increasing altitude. This impression agrees with the consensus reached in the earlier studies by Bolin (1950), Smagorinsky (1953) and Döös (1962). However, it does not agree with the recent result obtained by Sankar-Rao (1965) and Sankar-Rao and Saltzman (1969). Using a simple quasi-geostrophic framework, Sankar-Rao (1965) computed the effects (on the atmospheric motion) of the lifting of a latitudinally uniform zonal current of air by a realistic continental elevation. (In his study, the shape of the continental elevation is represented by 0th to 15th degree spherical harmonics). Although the computed response had significant magnitude, it hardly resembles the actual distribution of the stationary flow field in winter. These results of Sankar-Rao seem to be quite different from those of the present study which suggests the importance of mountains for maintaining the stationary disturbances observed in the upper troposphere and the stratosphere. The difference may be due to the phenomenon of quasi-resonance. Sankar-Rao pointed out that his solution is affected very much by quasi-resonance which takes place when the wavelength of the free atmospheric mode coincides with the characteristic scale of the mountains. In their study of the effects of orography, Charney and Eliassen (1949) adjusted the drag coefficient such that it was large enough to suppress the

phenomenon of quasi-resonance and so obtained realistic results. Quasi-resonance may not be a significant phenomenon in a general circulation model of the atmosphere in which the effects of nonlinear interaction among large-scale eddies and the effects of subgrid viscosity are incorporated in addition to the effects of surface friction considered in Sankar-Rao's theoretical model.

Following the study described above, Sankar-Rao and Saltzman (1969) evaluated the response of a quasi-geostrophic atmosphere to idealized heating. Based upon this study, Saltzman (1968) concluded that a good deal of the variance of the mean state in mid-latitudes is already explainable by asymmetric surface heating. However, the results of the present study indicate that thermal effects do not account for the essential features of the flow field in the upper troposphere and the stratosphere. The difference between the two results may be caused by the difference in the vertical distribution of the heating rate. In Fig. 4.7, the vertical profiles of the heating rate used by Sankar-Rao and Saltzman (1969) in their theoretical study are shown. For the sake of comparison, the vertical profile of the rate of heating due to dry and moist convection and condensation at 45N of the NM-model is added to the figure. The contribution of radiative cooling is not included in this heating rate because it has little longitudinal variation in the model atmosphere and may not affect the amplitude of stationary disturbances directly. (The latitude-height distribution of the rate of heating in the M-model may be found in Fig. 4.8). The heating profile adopted for the final result of Sankar-Rao and Saltzman (1969) is shown by the curve labeled  $\gamma=0.75$ . Accordingly, the relative magnitude of the heating rate in the upper troposphere of their model is larger than the correspond-

ing rate for the NM-model. As is evident from the results of Sankar-Rao and Saltzman, the excessive heating rate tends to increase the relative magnitude of the response of the upper tropospheric flow field to the heating. This is probably the reason why they get a realistic variance of the mean state by the thermal effect alone, whereas the variance of the meridional component of the stationary wind is relatively small in the upper troposphere of the NM-model. There are other differences in the computation of heating rate. Sankar-Rao and Saltzman assumed that the atmospheric heating is proportional to the air-sea (land) temperature difference. In the model atmosphere used for the present study, the heat of condensation and sensible heat flux are computed by more explicit methods as described in Section 2. Therefore, even if the horizontal distribution of heating determined in their study is significantly different from the heating in the NM-model atmosphere, it is not surprising.

So far, we have speculated why the relative importance of the effects of thermal heating in determining the stationary flow field in the upper troposphere differs between our numerical model and that of Sankar-Rao and Saltzman. In order to pinpoint the real cause for this difference, it is necessary to carry out more numerical experiments and theoretical studies designed for this purpose.

Finally, it should be pointed out here that an important ambiguity exists when one tries to determine the effect of heating upon the large-scale flow field based upon the results from numerical experiments such as those described in this study. As Fig. 4.3 indicates, mountains alter the thermal forcing by modifying the distributions of precipitation and the sensible heat flux from the earth's surface. In other words, the distribution of heating in the M-model is not the same as that of the NM-model. Therefore, one cannot separate the influences of thermal forcing from those of orography upon the circulation in a model atmosphere. These two effects interact with each other.

#### b. Southern Hemisphere

The time-mean distributions of the geopotential heights of isobaric surfaces in the Southern Hemisphere of both models are compared with those in the actual atmosphere in Fig. 4.9. According to this comparison, the agreement between the computed and the observed is poor. At the 1000-mb level of the actual atmosphere, a belt of large pressure gradient is located at 40-60S indicating the predominance of strong surface westerly winds around these latitudes (the so-called roaring forties). This important feature is almost missing from both model atmospheres. Accordingly, sea level pressure of the model atmospheres is not very realistic. As pointed out in Section 3C, this difficulty may be related to the systematic error involved in the finite-difference computation of the pressure gradient force. This error

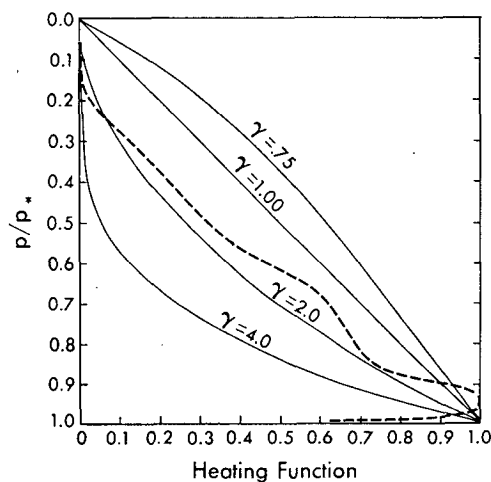


FIG. 4.7. Vertical profiles of the heating function adopted in the theoretical study of Sankar-Rao and Saltzman (1969), solid lines, and the vertical profile of zonal mean heating rate along 45N of the NM-model, dashed line. Here, the heating rate implies the rate of heating of the atmosphere due to moist convection, condensation and sensible heat flux from the earth's surface.

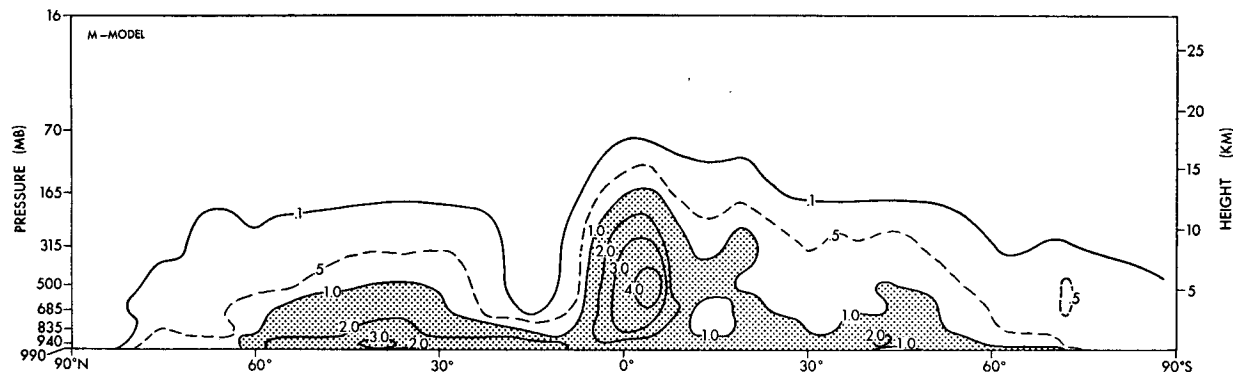


FIG. 4.8. Latitude-height distribution of the zonal mean rate of net heating ( $^{\circ}\text{K day}^{-1}$ ) due to moist convection, condensation and vertical mixing in the M-model atmosphere.

seems to become very serious in areas of steep topography such as the Andes and Antarctica. Therefore, it is desirable to reexamine the effect of mountains, particularly in the Southern Hemisphere, after this bias is removed from the model. At the 500-mb level the geopotential height field is close to axial-symmetric in both the actual and the model atmospheres. This result is consistent with the fact that a large-scale mountain range which could maintain stationary disturbances is missing in the Southern Hemisphere except in the polar region.

## 5. Cyclogenesis

It has been pointed out that cyclones tend to form in the lee of major mountain ranges such as the Tibetan Plateau and the Rocky Mountains (e.g., Pettersen, 1956). In order to determine how mountain ranges affect the frequency of cyclogenesis in the model atmosphere, a survey of the frequency of cyclogenesis was made for both M- and NM-atmospheres; the results are shown in Fig. 5.1. In this figure the locations of cyclogenesis are identified by black dots and the trajectories of cyclone centers are indicated by streaklines. If a low center emerges in the map of sea level pressure with a contour interval of 2.5 mb, it is regarded as cyclogenesis. The period of the analysis is 45 days for both models, and cyclones which already existed at the beginning of the period are excluded. The comparison between the results from the M-model and those from the NM-model indicate that major mountain ranges such as the Rocky Mountains or the Tibetan Plateau significantly increase the frequency of cyclogenesis in their lee.

In order to show the comparison between the distribution of the frequency of cyclogenesis in the M-model atmosphere and that in the actual atmosphere, we show in Fig. 5.2 the observed percentage frequency of cyclogenesis and of cyclone centers in winter (Pettersen, 1956). In general, the streakline map of the M-model shown in Fig. 5.1 compares favorably with the cyclo-

genesis and cyclone center maps of Fig. 5.2 except in the lee of the European Alps which is too small to be resolved by the finite-difference grid of the M-model. An attempt to examine the statistics of cyclogenesis in a model atmosphere has been made by Miyakoda *et al.* (1972), who pointed out that the area of frequent cyclogenesis in their numerical weather prediction model agrees with those in the actual atmosphere. The present results suggest that mountains play a major role in determining the geographical distribution of cyclogenesis in the atmosphere.

Lee cyclogenesis is usually considered to be primarily a consequence of vertical stretching of air columns associated with the downslope motion at the earth's surface. Analyzing the evolution of the circulation during the period of lee cyclogenesis, Newton (1956) obtained a somewhat more sophisticated picture of the phenomenon. He found that cyclogenesis took place when the region of the strongest upward motion at the 500-mb level, directly beneath the upper-tropospheric jet stream, became superimposed over the band of maximum vertical stretching in the lower troposphere. It should be pointed out, however, that most of cyclogenesis in the lee of the Tibetan Plateau takes place off the coast of southern China where downslope motion does not exist. Therefore, one has to consider other mechanisms in order to account for this type of cyclogenesis. As pointed out by Bolin (1950) and confirmed by the present study, a mountain tends to increase the intensity of the jet stream on the southeastern side of the first lee trough downstream. It is highly probable that the increased baroclinicity due to this intensification of the jet stream is partly responsible for the enhancement of cyclogenesis in the lee of major mountain ranges, i.e., over the South China Sea and the southeastern United States. Another important factor which may influence the genesis and the development of cyclones is airmass modification. In the preceding section, it is pointed out that mountains intensify and shift northward the anticyclone over the Eurasian continent and are responsible for the maintenance of

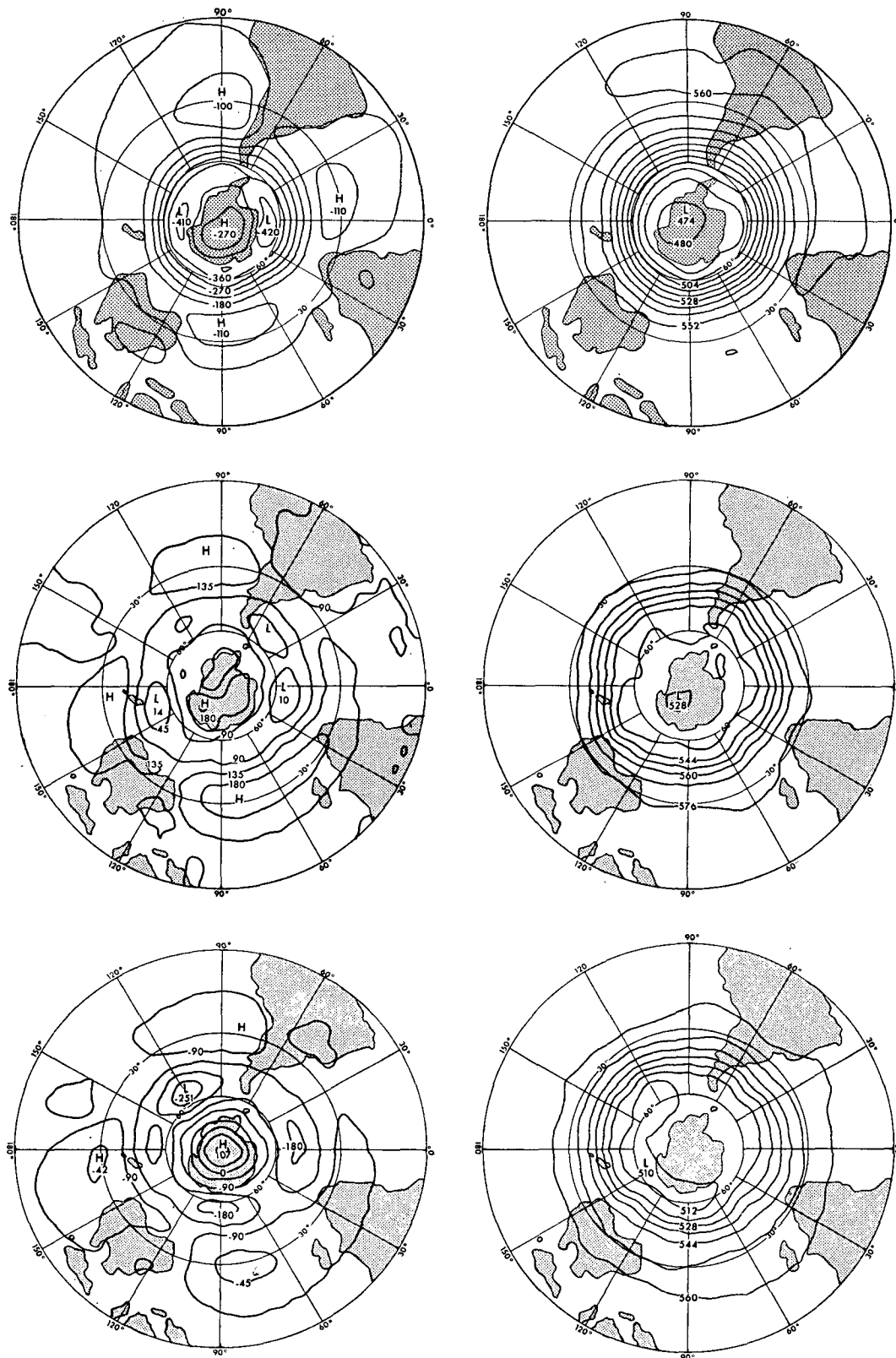


FIG. 4.9. Time-mean geopotential height maps at 1000 mb (left) and 500 mb (right) in the Southern Hemisphere. Units for 1000-mb case: geopotential meters; for 500-mb case: geopotential decameters. Top, observed (Taljaard *et al.*, 1969); middle, the M-model; bottom, the NM-model.

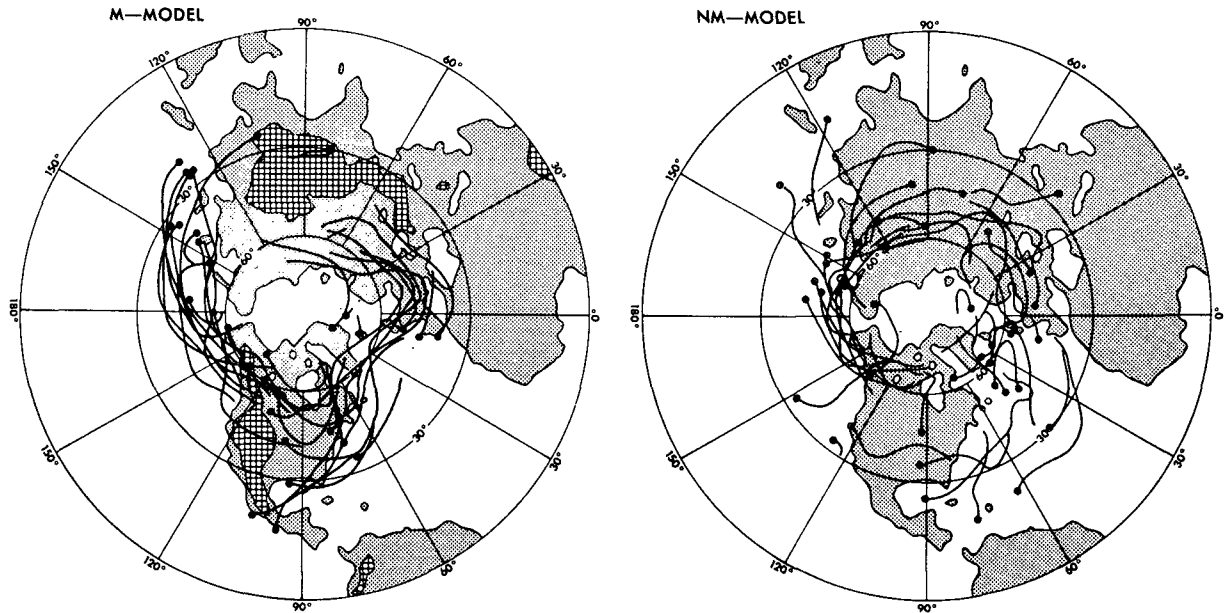


FIG. 5.1. Computed streaklines of cyclones. Black dots indicate the approximate locations of cyclogenesis. The analysis period is 45 days for both models. Right side, the NM-model; left side, the M-model.

the Siberian high. The outflow of cold air along the periphery of the Siberian high enhances the modification of the air mass off the east coast of China (Fig. 4.3) and may influence the genesis and the development of cyclones in this general area. Obviously, some of this discussion is based upon speculation. In order to study how mountains actually influence cyclogenesis, synoptic analyses of the mechanism of cyclogenesis must be made in the model as well as in the actual atmosphere.

### 6. Transports by large-scale eddies

The results of Section 3d indicate that the topography of the earth's surface significantly alters the distribution of eddy kinetic energy between the stationary and the transient disturbances. In this Section, we consider how mountains affect the relative importance of stationary and transient eddies in transporting various quantities such as heat, angular momentum and moisture. In

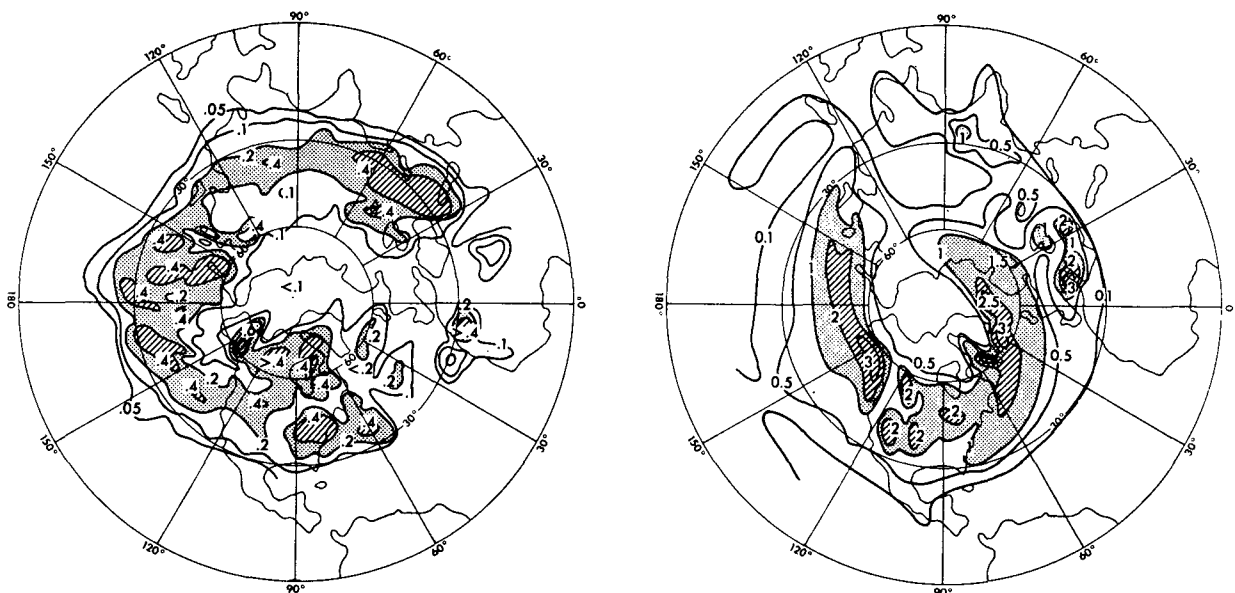


FIG. 5.2. Left: Observed percentage frequency of cyclogenesis in winter. Right: observed percentage frequency of cyclone centers in winter. The frequencies refer to areas of 100,000 km<sup>2</sup> over the period 1899-1939. (After Petterssen, 1956.)

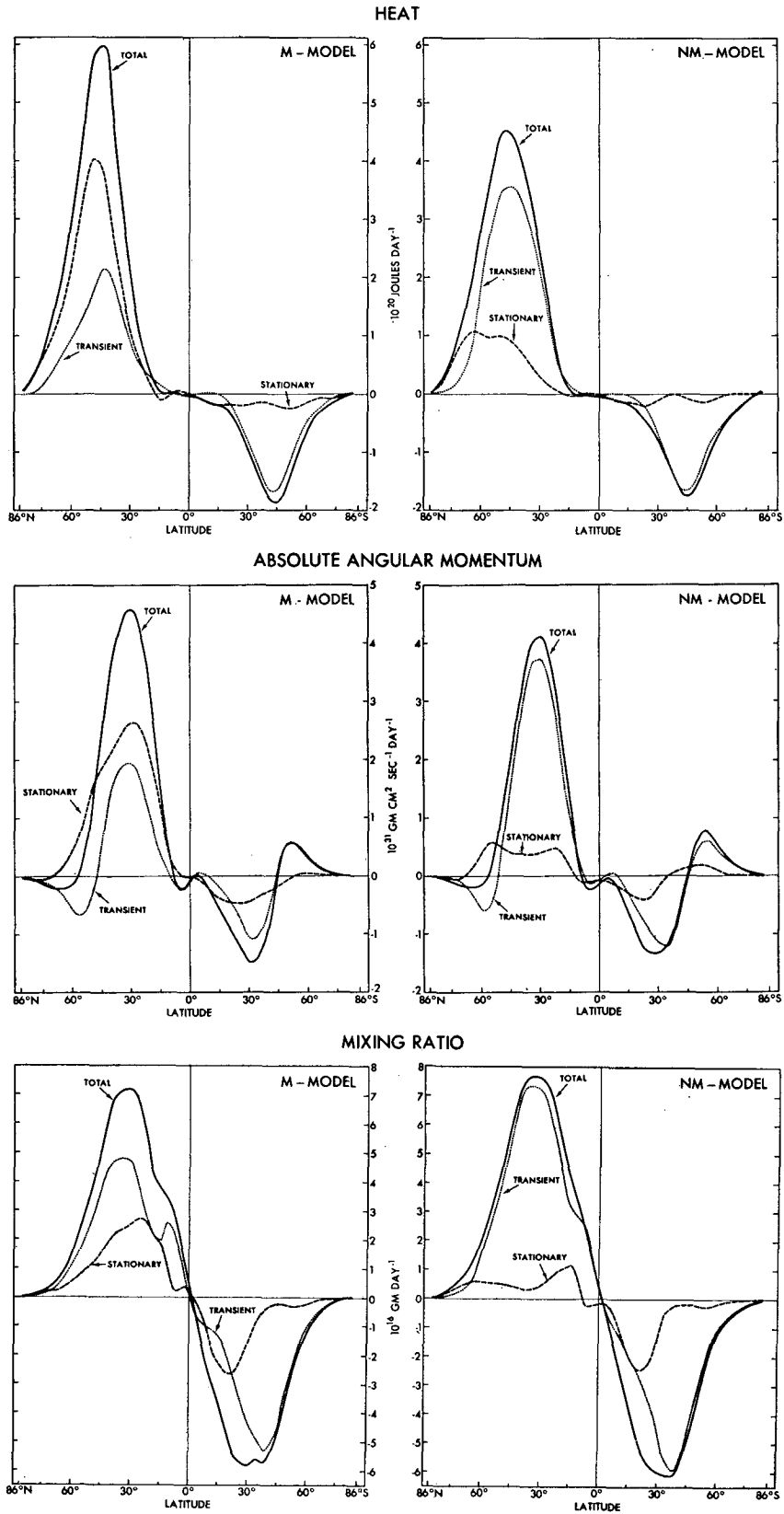


FIG. 6.1. Northward eddy transport (vertical integral) of heat (top) in units of  $10^{20}$  J day $^{-1}$ , angular momentum (middle) in units of  $10^{31}$  gm cm $^{-2}$  sec $^{-1}$  day $^{-1}$ , and moisture (bottom) in units of  $10^{18}$  gm day $^{-1}$ . Left, the M-model; right, the NM-model.



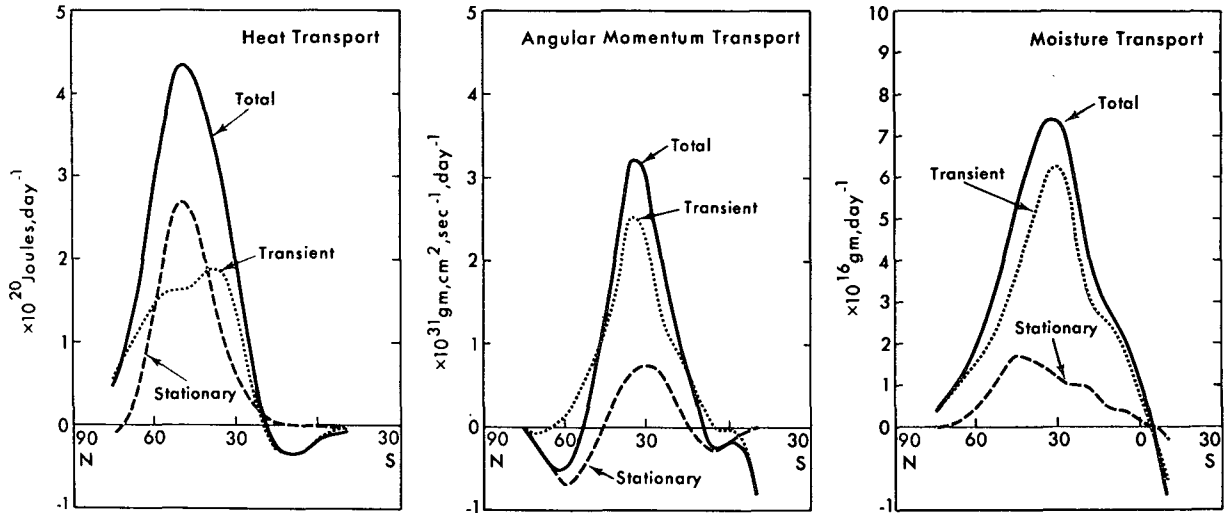


FIG. 6.2. Observed average over five Januaries of northward eddy transport of heat (left), angular momentum (center) and moisture (right). (After Oort and Rasmusson, 1971.)

Fig. 6.1, the latitudinal distributions of the northward transport of these quantities due to each eddy component are shown for both M- and NM-models. Here, the stationary and the transient components of the northward transport of a quantity  $r$  are defined by  $2\pi a \cos\theta(\bar{v}^*r^*)$  and  $2\pi a \cos\theta[(v')^*(r')^*]$ , respectively ( $a$  is the radius of the earth and  $\theta$  the latitude). This figure clearly indicates that, in general, the effects of mountains increase the northward transports of various quantities by stationary eddies but decrease the transport by transient eddies. Accordingly, the total north-

ward eddy transport, i.e., the sum of the contribution from both eddies, is altered less than the change in transport by each eddy component. The effects of mountains upon the eddy transports described above are particularly evident in the Northern Hemisphere which is occupied by large-scale major mountain ranges.

Fig. 6.1 indicates that, in the Northern Hemisphere M-model atmosphere, heat transport by stationary eddies is larger than that by transient eddies. Since the eddy kinetic energy of stationary disturbances is less than that of transient disturbances (see Fig. 3.4), this

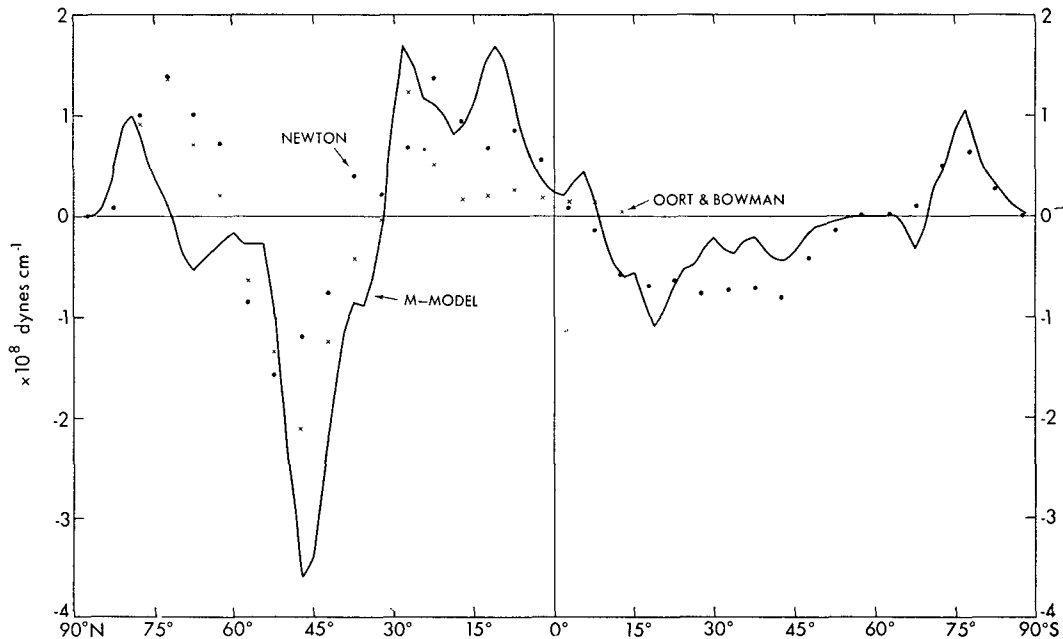


FIG. 7.1. Latitudinal distribution of mountain torque. The estimates of actual torque by Newton (1971) and Oort and Bowman (1974) are indicated by dots and crosses, respectively. Solid line, M-model.

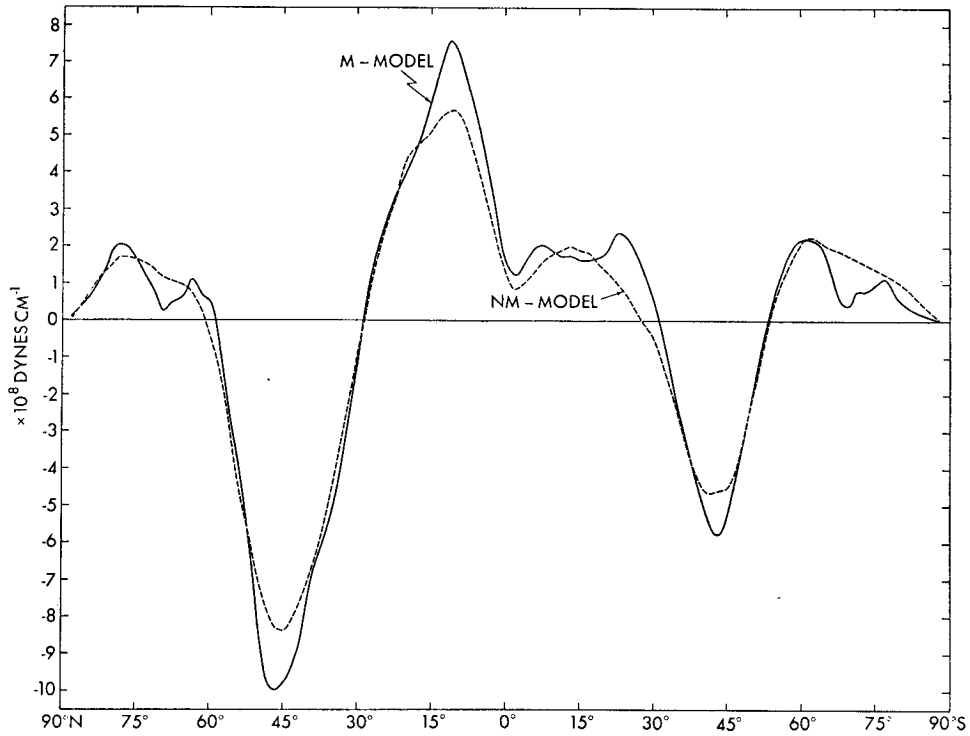


FIG. 7.2. Latitudinal distribution of total torque, i.e., the sum of surface torque and mountain torque. Solid line, the M-model; dashed line, the NM-model.

result suggests that stationary disturbances transport heat more efficiently than transient ones. If one compares the longitude-height cross section of the time-mean distribution of meridional wind along 45N (Fig. 4.5) with that of the temperature anomaly along the same latitude circle, shown in Fig. 4.6, one finds that the cold anomaly around 135E occupies the region of strong northerly flow, whereas the warm anomaly

around 135W coincides with the region of southerly flow. (This result is consistent with the westward tilt of the stationary trough mentioned in Section 4a5.) Since there is a positive correlation between the temperature anomaly and the meridional component of wind, stationary disturbances transport heat poleward very effectively in the Northern Hemisphere.

In his theoretical study, Bolin (1950) pointed out

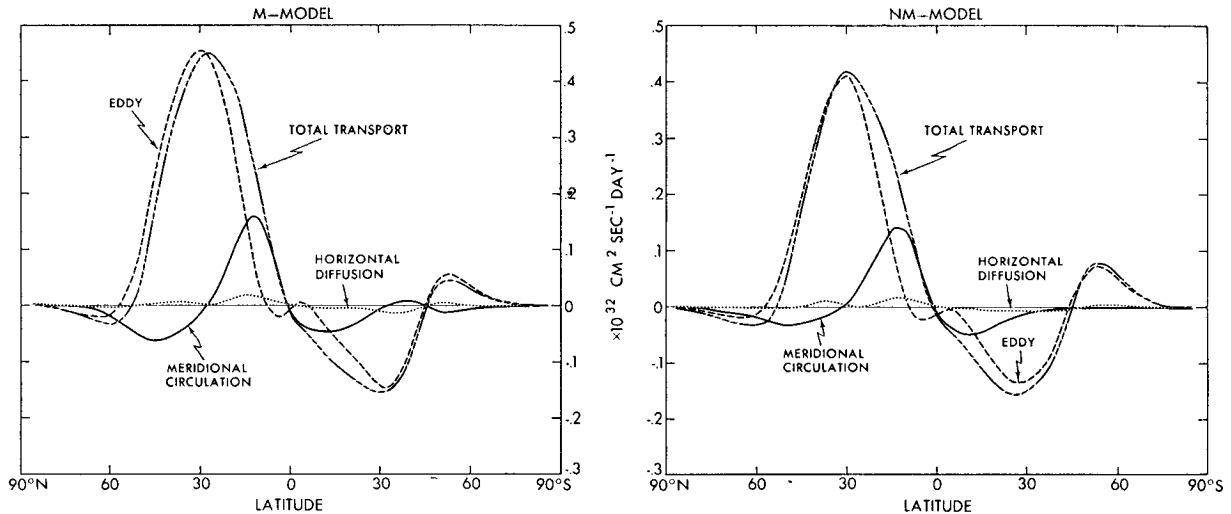


FIG. 7.3. Latitudinal distribution of the northward transport of absolute angular momentum: dashed line, eddy; solid line, meridional circulation; dotted line, horizontal diffusion; solid-then-dashed line, total. Left side, the M-model; right side, the NM-model.

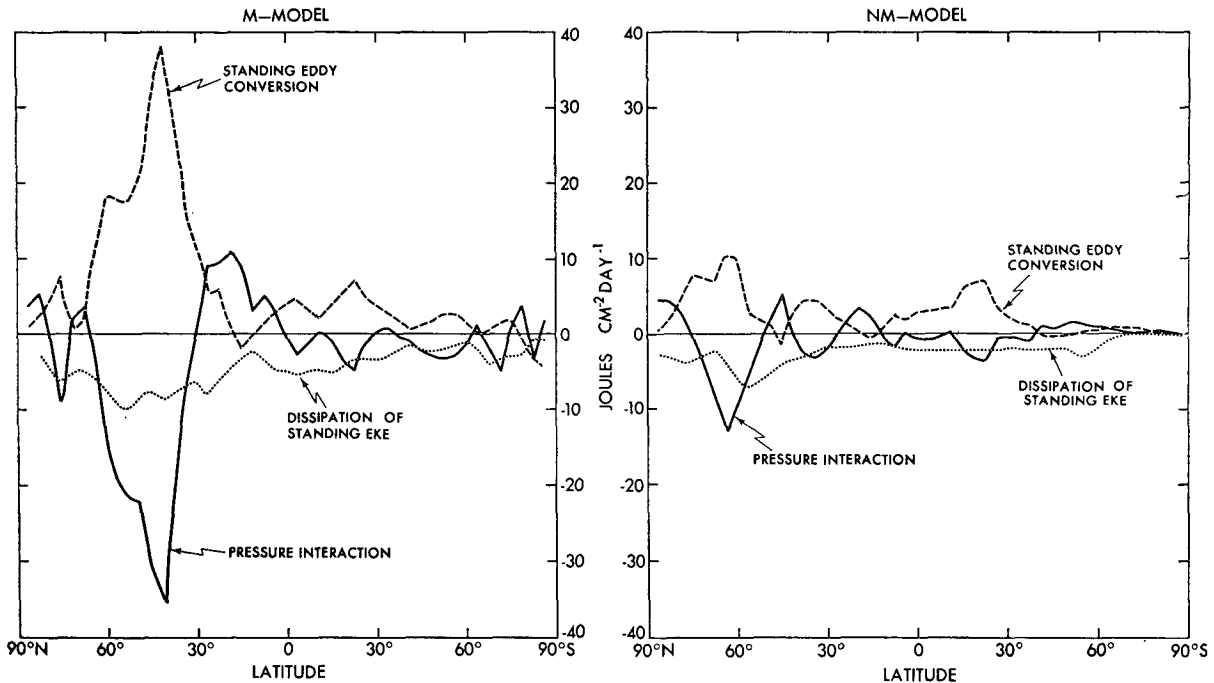


FIG. 8.1. Latitudinal distribution of various components of the budget of eddy kinetic energy of stationary disturbances in the M-model (left) and the NM-model (right) troposphere. Here the troposphere is defined as the part of the atmosphere below the 240-mb level. Dashed line, stationary eddy conversion; dotted line, dissipation; solid line, pressure interaction.

that the trough of the stationary disturbance generated in the lee of a circular mountain tends to tilt from southwest to northeast and thus transports angular momentum poleward. Similar tilting of the trough is evident in the time-mean map of geopotential height of the 500 and 300-mb surfaces in the M-model atmosphere shown in Fig. 4.1. Accordingly, stationary disturbances in the M-atmosphere transport angular momentum poleward. The comparison between the latitudinal distribution of eddy kinetic energy (Fig. 3.4) and that of angular momentum transport in the M-model atmosphere (Fig. 6.1) reveals that stationary eddies transport angular momentum more effectively than transient eddies do. Stationary disturbances also transport moisture poleward. However, the transport by stationary eddies is significantly less than that of transient eddies. Comparison of Figs. 6.1 and 3.4 indicates that the former is as efficient as the latter.

According to the comparison between the eddy transports in the M-model atmosphere and those in the actual atmosphere<sup>5</sup> shown in Fig. 6.2, the transport by stationary disturbances is too large whereas that by transient disturbances is too small in the M-model atmosphere. This result may be consistent with the fact that the kinetic energy of stationary eddies is too large but that of transient eddies is much too small in the M-model atmosphere. It should be noted,

<sup>5</sup> Note that the definition of the transient component of eddy transport used by Oort and Rasmusson (1971) is slightly different from that adopted in this study.

however, that the heat transport by stationary disturbances in the actual atmosphere is also so efficient that it is larger than the transient eddy transport in certain latitudes even though the kinetic energy of stationary disturbances is much smaller than that of transient disturbances.

## 7. Angular momentum budget

White (1954) and Widger (1949) showed that mountain torque in the Northern Hemisphere, though generally smaller than frictional torque, is of the same order of magnitude and thus cannot be neglected. The latitudinal distribution of the mountain torque in the M-model atmosphere<sup>6</sup> is shown in Fig. 7.1 together with the estimates of this quantity in the actual atmosphere by Newton (1971) and Oort and Bowman (1974). In the Northern Hemisphere of the M-model, the mountain torque is positive in both high and low latitudes but has large negative values in middle latitudes in qualitative agreement with the estimates of the actual mountain torque by Newton and Oort and Bowman. In the Southern Hemisphere, it is negative in middle and low latitudes and is positive in very high latitudes. In general, the mountain torque in the Southern Hemisphere, which is covered mostly by oceans, is

<sup>6</sup> This mountain torque is computed from the vertical mass integral of the pressure gradient force because the conventional method of evaluating mountain torque yields unreasonable results in the latitude belt of the steep Andes Mountain ranges. For further details, see Appendix B.

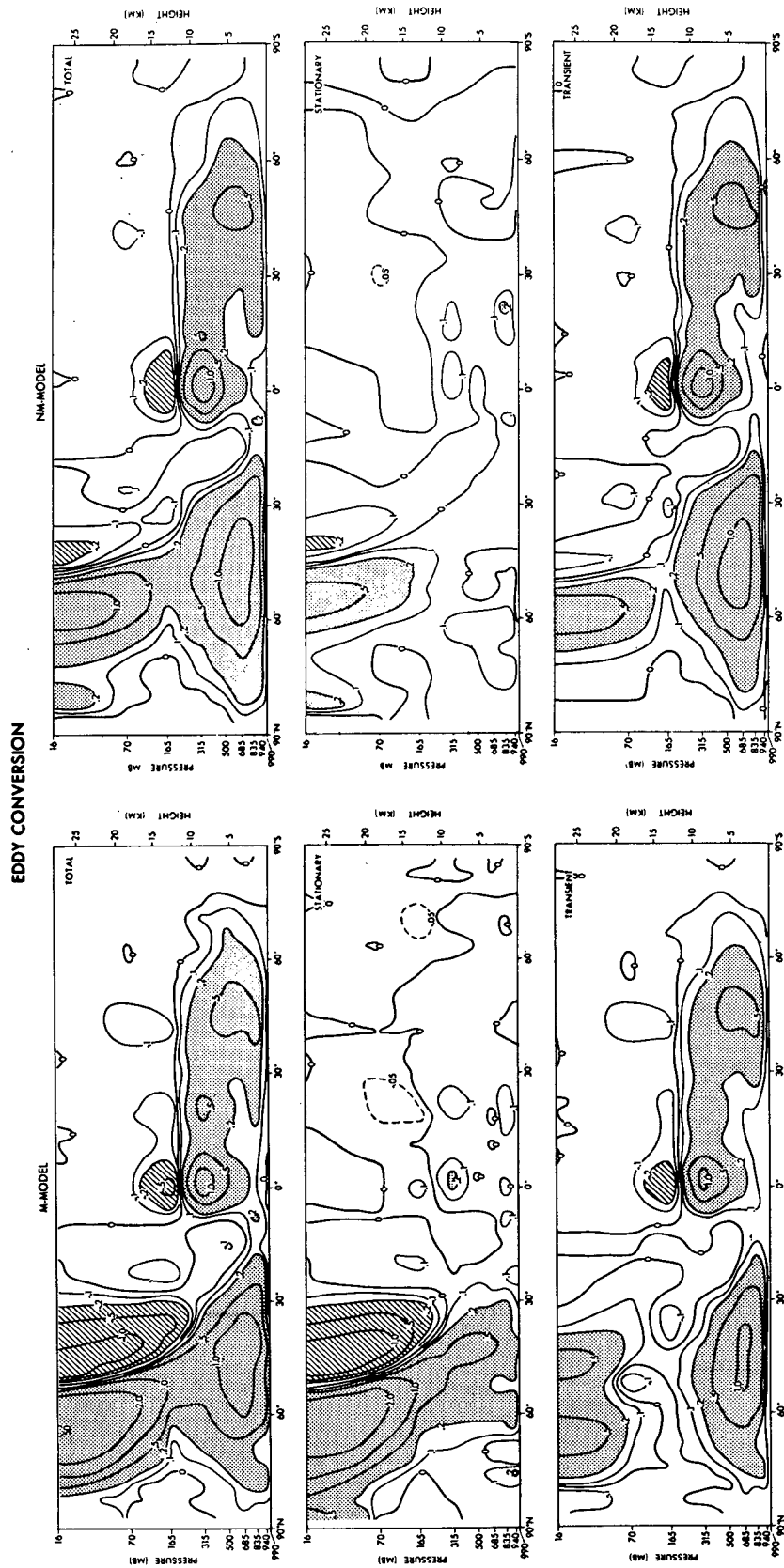


FIG. 8.2. Latitude-height distribution of eddy conversion: left, the M-model; right, the NM-model. Top, total; middle, stationary; bottom, transient. Units:  $10^{-1} \text{ J cm}^{-2} \text{ mb}^{-1} \text{ day}^{-1}$ .

considerably smaller than that in the Northern Hemisphere which is occupied by major mountain ranges.

Mountains influence the angular momentum budget of the atmosphere through mountain torque. They also change the torque due to surface wind stress by altering the surface wind vectors. In order to show the net effect of topography upon the distribution of total torque, Fig. 7.2 compares the latitudinal distribution of total torque in the M-model with that in the NM-model. According to this comparison, the net effect of orography upon the latitudinal distribution of total torque is not negligible but relatively small in the model with the insolation of perpetual January.

In a quasi-steady state, the total surface torque discussed above should be compensated by the effects of angular momentum transport by atmospheric motion. Fig. 7.3 shows the latitudinal distributions of the northward transport of angular momentum due to various components of flow in the model atmosphere. This figure clearly indicates that not only the transport by large-scale eddies but also that by meridional circulation is affected little by mountains. Particularly, the distribution of the net transport due to all components in the M-model atmosphere coincides very well with the corresponding distribution in the NM-atmosphere. This indicates again the smallness of the effects of orography upon the overall balance of angular momentum.

## 8. Energetics

### a. Stationary disturbances in the troposphere

Assuming the hydrostatic relationship, the equation describing the budget of kinetic energy of stationary eddies is given by

$$\left[ \bar{\mathbf{V}}^* \cdot \frac{\partial \bar{\mathbf{V}}^*}{\partial t} \right] = - \left[ \bar{\mathbf{V}}^* \cdot \left( \mathbf{V} \cdot \nabla_H + \omega \frac{\partial}{\partial p} \right)^* \right] - [\bar{\omega}^* \bar{\alpha}^*] - [\bar{\mathbf{V}}^* \cdot \nabla_H \bar{\phi}^*] + [\bar{\mathbf{V}}^* \cdot \bar{\mathbf{F}}^*] = 0. \quad (8.1)$$

In these equations,  $\mathbf{V}$ ,  $\nabla_H$ ,  $\phi$ ,  $t$  and  $\mathbf{F}$  are the horizontal wind vector, horizontal nabla operator, geopotential height of isobaric surface, time, and horizontal frictional force due to subgrid-scale eddies, respectively. For the definitions of zonal and time mean operators,  $[\ ]$  and  $(\ )$ , and that of the deviations from zonal means,  $(\ )^*$ , see the first paragraph of Section 3d. The second term on the right-hand side of (8.1) may be subdivided further as

$$- [\bar{\mathbf{V}}^* \cdot \nabla_H \bar{\phi}^*] = - [\bar{\omega}^* \bar{\alpha}^*] - \left[ \nabla_H \cdot (\bar{\mathbf{V}}^* \bar{\phi}^*) + \frac{\partial}{\partial p} (\bar{\omega}^* \bar{\phi}^*) \right], \quad (8.2)$$

where  $\omega$ ,  $\alpha$  and  $p$  denote vertical  $p$ -velocity, specific volume of air and pressure, respectively. Combining

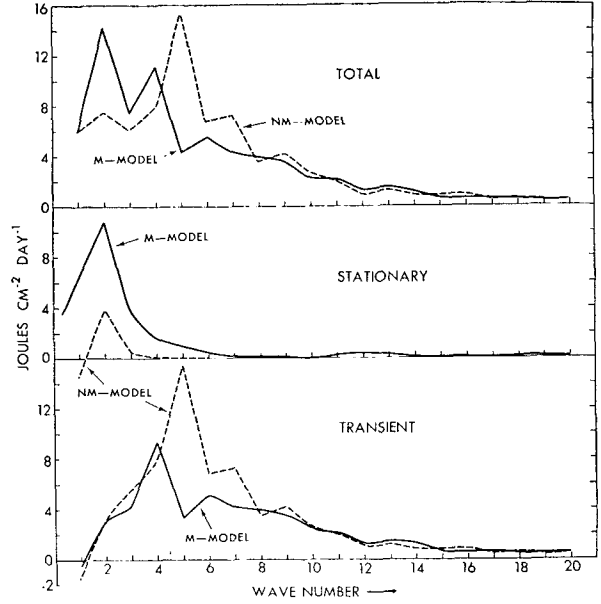


FIG. 8.3. Spectrum of the vertical mass integral of eddy conversion for the latitude belt between 40 and 50N: solid line, M-model; dashed line, NM-model. Top, total; middle, stationary; bottom, transient. The vertical integral includes both the stratosphere and the troposphere.

(8.1) and (8.2), we have

$$\left[ \bar{\mathbf{V}}^* \cdot \frac{\partial \bar{\mathbf{V}}^*}{\partial t} \right] = - \left[ \bar{\mathbf{V}}^* \cdot \left( \mathbf{V} \cdot \nabla_H + \omega \frac{\partial}{\partial p} \right)^* \right] - [\bar{\omega}^* \bar{\alpha}^*] - \left[ \nabla_H \cdot (\bar{\mathbf{V}}^* \bar{\phi}^*) + \frac{\partial}{\partial p} (\bar{\omega}^* \bar{\phi}^*) \right] + [\bar{\mathbf{V}}^* \cdot \bar{\mathbf{F}}^*] = 0. \quad (8.3)$$

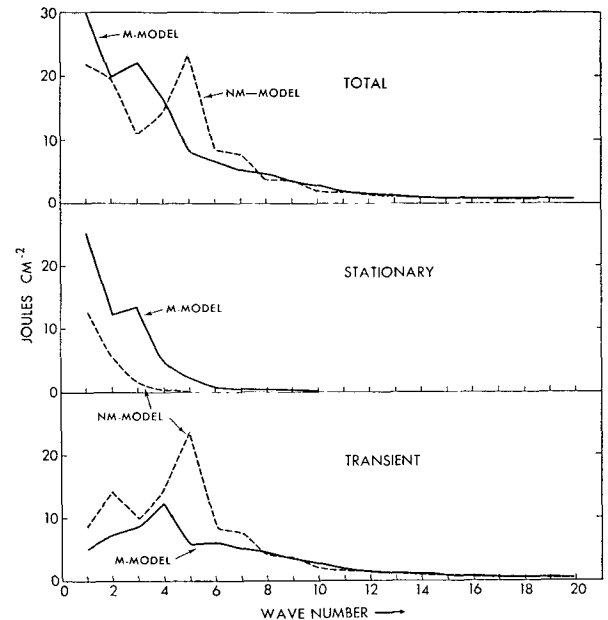


FIG. 8.4. As in Fig. 8.3 except for eddy kinetic energy.

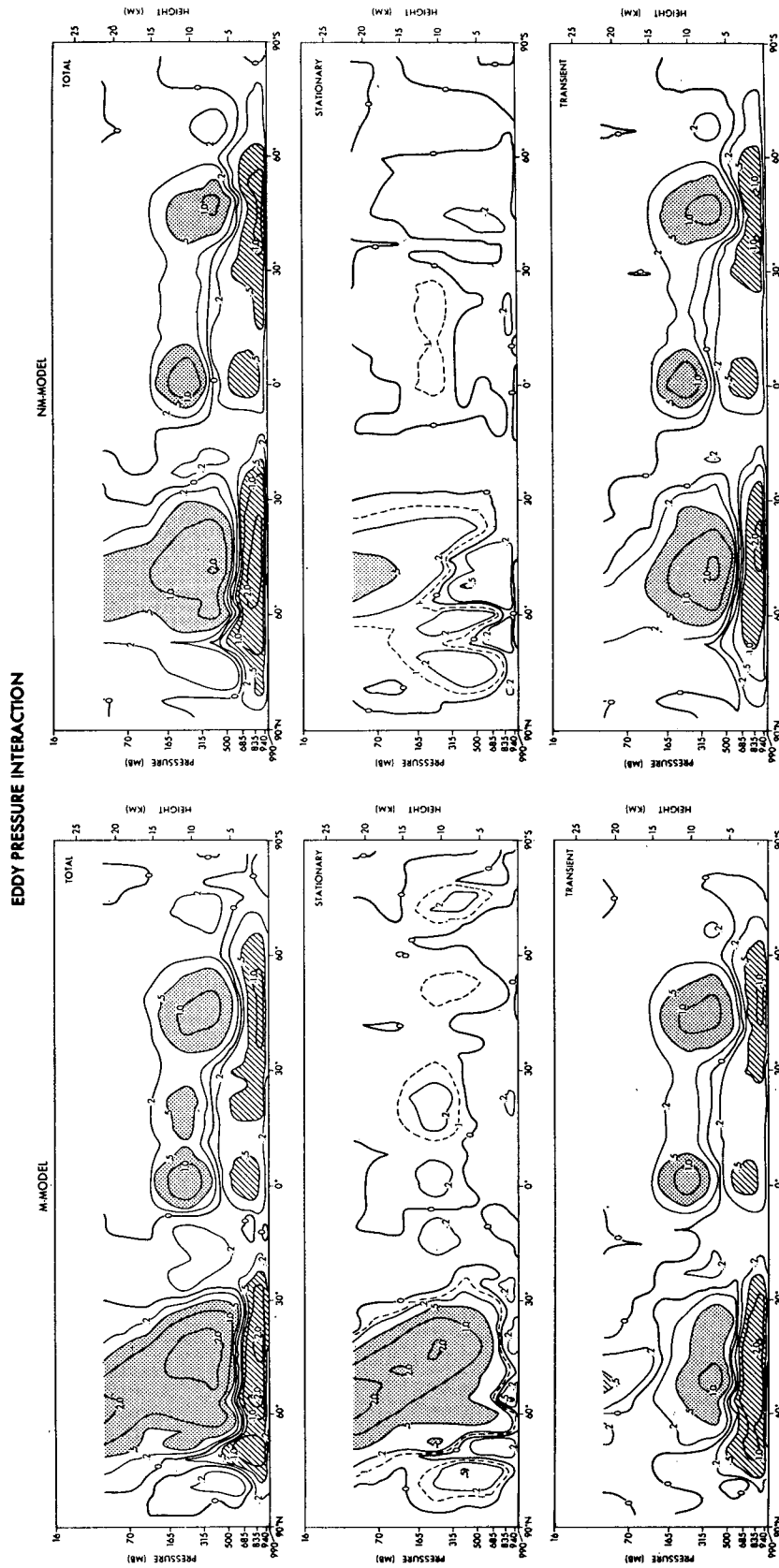


FIG. 8.5. Latitude-height distribution of the vertical component of eddy pressure interaction: left side, M-model; right side, NM-model. Top, total; middle, stationary; bottom transient. Units,  $J \text{ cm}^{-2} \text{ day}^{-1}$ .

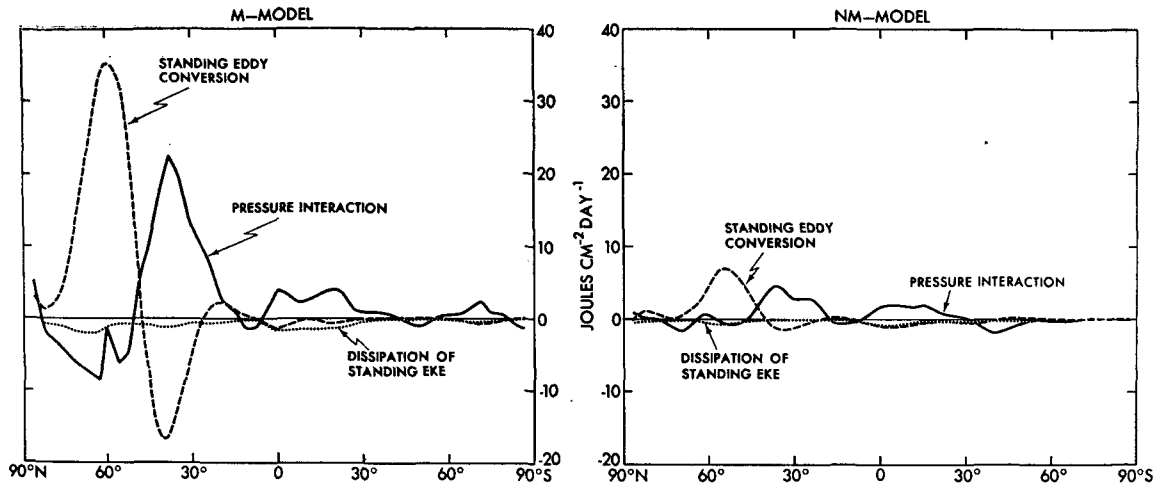


FIG. 8.6. Latitudinal distribution of various components of the budget of eddy kinetic energy of stationary disturbances in the M-model (left) and the NM-model (right) stratosphere. Here the stratosphere is defined as the part of the atmosphere above the 240-mb level. Dashed line, stationary eddy conversion; dotted line, dissipation; solid line, pressure interaction.

The first term in the right-hand side of (8.3) represents the contribution of the energy exchange between stationary eddies and other components of flow such as transient eddies and zonal currents. The second term denotes the conversion of potential energy into the kinetic energy of stationary disturbances, the third term represents the energy exchange with the surroundings through pressure interaction, and the fourth term represents the contribution of dissipation.

In order to show how the energetics of stationary disturbances in the model troposphere is affected by the effects of mountains, we present in Fig. 8.1 the latitudinal distributions of three of the four components of the energy budget identified in (8.3). The left and right parts of the figure represent the distribution for the M- and the NM-models, respectively. According to this comparison, the rate of stationary eddy conversion increases markedly in the middle latitudes of the Northern Hemisphere resulting from the incorporation of the effects of mountains into the model. This is probably the major reason why the kinetic energy of stationary disturbances increases due to mountain effects. In his observational study, Holopainen (1970) estimates how mountains influence the mass integral of the first term of (8.4) through boundary forcing. Based upon his analysis, he concluded that the effect of mountains upon the energy budget of stationary disturbances is small. Unfortunately, it was not possible to compute the first term before the dismantling of the computer used for this study. Nevertheless, the present results indicate the profound effects of mountains upon the energetics of stationary eddies in the model troposphere, particularly on the rate of stationary eddy conversion.

The increase of the stationary component of eddy conversion mentioned above is accompanied by the increase of the energy transfer from zonal to eddy

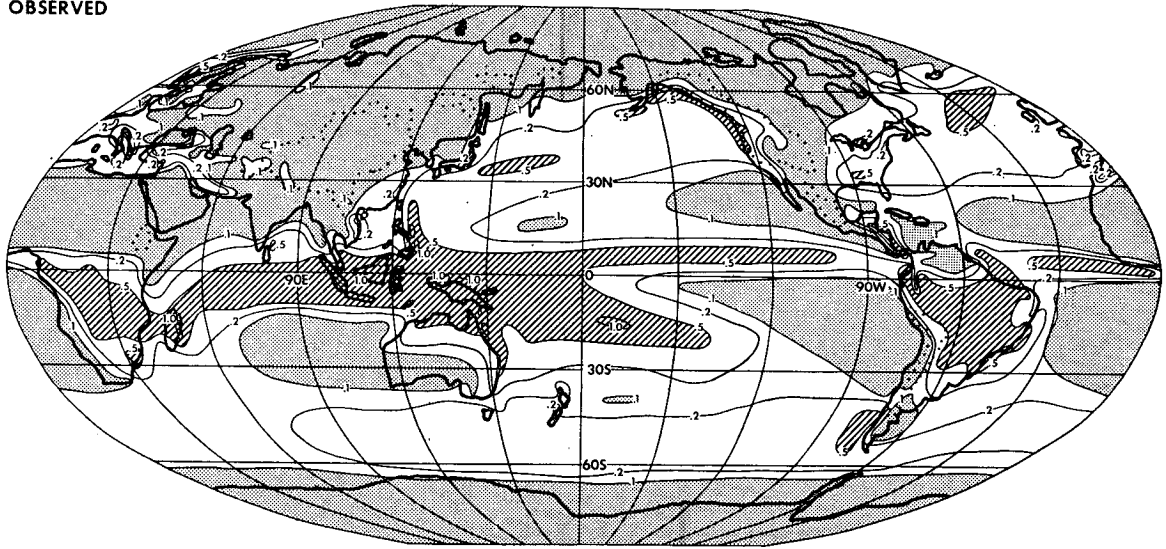
available potential energy. This is underscored by the fact that the poleward transport of heat by stationary eddies increases markedly due to the effect of mountains (see Section 6).

Fig. 8.1 also reveals that mountains influence not only the rate of eddy conversion but also the stationary component of pressure interaction. The pressure interaction is responsible for removing the energy from middle latitudes to low latitudes in the Northern Hemisphere of the model. As discussed in the latter part of this section, it also transports large amounts of energy into the stratosphere of the Northern Hemisphere and plays an important role in maintaining the kinetic energy of stationary disturbances there.

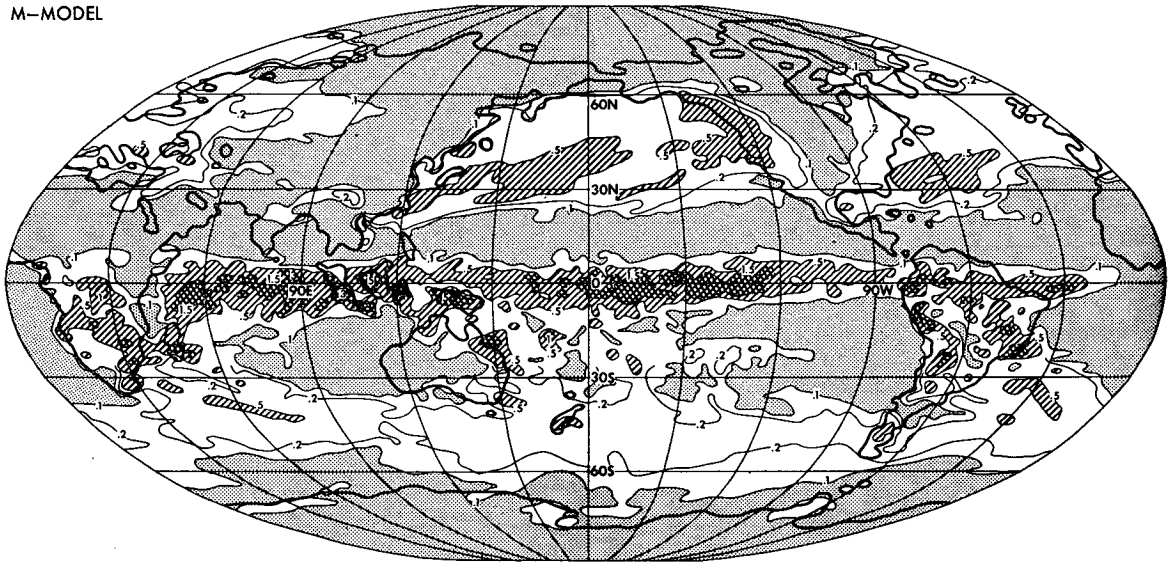
The remarkable increase of stationary eddy conversion in the Northern Hemisphere of the model resulting from the incorporation of the effects of mountains is also evident in Fig. 8.2 in which the latitude-height distributions of total, stationary and transient eddy conversion in the M-model atmosphere are compared with those in the NM-model atmosphere. The figure also shows that the rate of transient eddy conversion decreases significantly in response to the increase of the stationary eddy conversion mentioned above. Because of this compensation, the total eddy conversion is affected little by the effects of mountains in the model troposphere. A similar tendency of compensation is evident between the kinetic energy of stationary eddies and that of transient disturbances as discussed in Section 3.

In order to examine how the longitudinal scale of eddy conversion in the atmosphere is affected by mountains, stationary and transient eddy conversion in both model atmospheres are subdivided into the contributions from different longitudinal wavenumbers. Fig. 8.3 shows the results of the analysis for the latitude belt ranging from 40 to 50N. According to this figure,

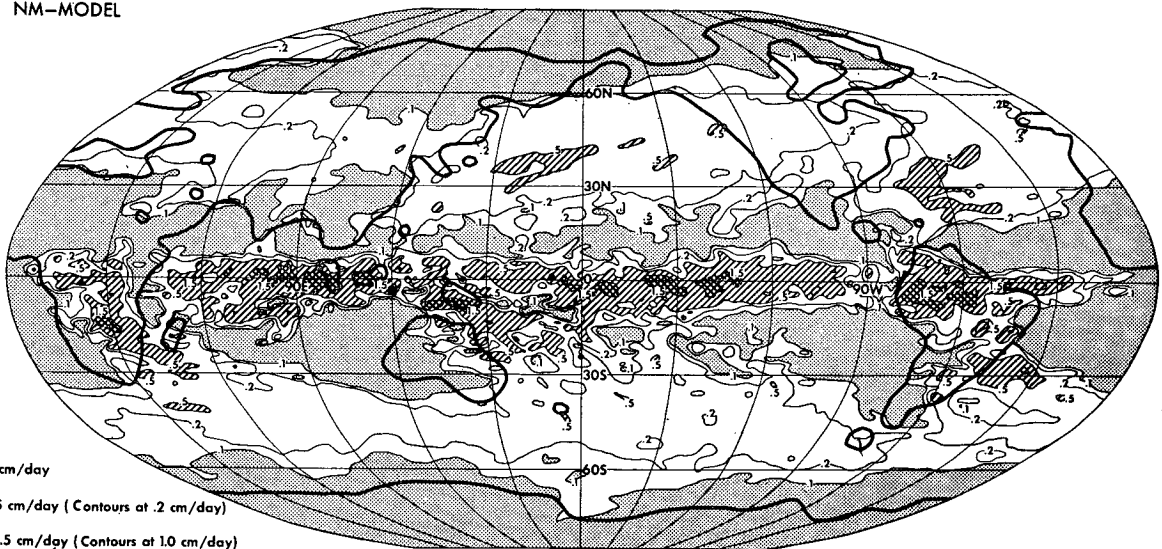
OBSERVED

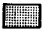
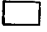




M-MODEL



NM-MODEL



-  < .1 cm/day
-  .1 to .5 cm/day (Contours at .2 cm/day)
-  .5 to 1.5 cm/day (Contours at 1.0 cm/day)
-  > 1.5 cm/day



mountains markedly increase the stationary eddy conversion which takes place at very low wavenumbers, i.e., 1-3. They also decrease the wavenumber of maximum transient eddy conversion from 5 to 4. Therefore, the longitudinal scale of total eddy conversion (sum of transient and stationary components) increases significantly as a result of incorporating the effects of mountains. Saltzman and Fleisher (1961) estimated the wavenumber spectrum of total eddy conversion in the actual atmosphere. Their results indicate that the maximum total eddy conversion takes place at wavenumbers which are smaller than the wavenumber of maximum baroclinic instability. Based upon their result, they speculated that mountains may be partly responsible for increasing the longitudinal scale of eddy conversion. Their speculation seems to be consistent with the present results.

In response to the increase in the characteristic scale of eddy conversion mentioned above, the scale of large-scale disturbances in the model atmosphere also increases when mountains are included in the model. Fig. 8.4 shows the wavenumber spectrum of eddy kinetic energy in both model atmospheres. Here eddy kinetic energy represents the vertical mass integral in the latitude belt ranging from 40 to 50N. This figure indicates that mountains significantly increase the kinetic energy of stationary eddies, which have very low wavenumbers, and contribute to the net increase of the characteristic scale of disturbances in the model atmosphere. It seems to be significant that the longitudinal scale of transient eddies also increases due to mountain effects. This increase is consistent with the similar increase in the scale of transient eddy conversion mentioned earlier.

#### *b. Stationary disturbances in the stratosphere*

It has been pointed out by Oort (1964) and others that the major source of kinetic energy of the stratospheric disturbances is the supply of energy from the troposphere through eddy pressure interaction. Fig. 8.5 shows the latitude-height distribution of the vertical component of eddy pressure interaction in both the M- and NM-atmospheres. The contributions of stationary, transient and total eddies are shown separately. In the Northern Hemisphere of the model, the energy exchange between the troposphere and the stratosphere through the stationary component of eddy pressure interaction increases appreciably as a result of incorporating the effects of mountains. On the other hand, the energy exchange through the transient component of eddy pressure interaction decreases somewhat. Since the increase of the stationary component is much larger than the decrease of the transient component, total eddy pressure interaction increases as described above. It should be noted that, in the M-model stratosphere,

most of the energy supplied from the troposphere is accomplished by the stationary component of eddy pressure interaction.

Fig. 8.3 reveals that the longitudinal scale of the stationary eddy conversion in the model troposphere is very large. Accordingly, the stationary component of eddy pressure interaction also has a large longitudinal scale, and the upward flux of energy due to this component does not attenuate with height as rapidly as the transient component. [See Charney and Pedlosky (1963) for the theoretical discussion of the attenuation of upward flux of energy.] Since the stationary eddy conversion in the model troposphere increases markedly due to the effects of mountains, the upward flux of energy due to stationary eddy pressure interaction also increases. This is why the energy supplied by the pressure interaction is so large in the M-model stratosphere as compared to the NM-model. The marked increase in the upward flux of energy resulting from the incorporation of mountains is noted by Washington (1973).

In addition to pressure interaction, conversion of potential energy into eddy kinetic energy plays an important role in the energy budget of the stratosphere of the winter hemisphere. As Fig. 8.2 indicates, the rate of stationary eddy conversion in the M model stratosphere increases markedly as a result of incorporating the effects of mountains. This increase in higher latitudes far offsets the contribution of the negative stationary eddy conversion which appears in lower latitudes. Recent observational studies of Dopplick (1971) indicate that in the high latitude region of the winter stratosphere, eddy conversion is often positive<sup>7</sup> in qualitative agreement with the results of the present study.

Fig. 8.6 shows the latitudinal distributions of three of the components of the budget of eddy kinetic energy of stationary disturbances in the stratosphere of both models. The three components are eddy conversion, pressure interaction and dissipation, as given on the right-hand side of (8.3). According to this figure, the influence of mountains upon the energetics of stationary disturbances is very large in the Northern Hemisphere, whereas it is small in the Southern Hemisphere of the model. As pointed out already, mountains markedly increase the rate of stationary eddy conversion in high latitudes. Also, they increase the contribution of pressure interaction in the middle latitudes and the subtropics of the Northern Hemisphere of the model. The contribution of dissipation is small in the stratosphere of both models. Nevertheless, it is much larger in the M-model than in the NM-model. If one adds up the contributions of these three components in the

<sup>7</sup> The positive eddy conversion is noted earlier by many authors (e.g., Reed *et al.*, 1963; Miyakoda, 1963; Mahlman, 1969).

FIG. 9.1. Global distribution of the mean rate of precipitation ( $\text{cm day}^{-1}$ ): top, observed (Möller, 1951); middle, the NM-model; bottom, the M-model.

M-model stratosphere, one gets large positive values in the high latitudes of the Northern Hemisphere. This positive value has to be compensated by another term which is not computed in this study i.e., energy exchange between stationary eddies and zonal currents or transient eddies.

## 9. Precipitation

The effects of mountains upon the global distribution of precipitation was discussed earlier by Manabe and Holloway (1970)<sup>8</sup> based upon the results from the model with low computational resolution. Since the basic features of their results are similar to the present results, a very brief description of the difference between the distribution of precipitation of the M-model and that of the NM-model is made here.

As is known, mountain ranges force upward motion and accordingly cause adiabatic cooling of air and induce precipitation. They also block air flow and markedly alter the way in which heat and moisture are transported. Therefore, it is expected that mountain ranges significantly affect the distribution of precipitation. However, Kasahara and Washington (1971) noted that the global distribution of precipitation of their model is hardly affected by mountains. In this respect, their results differ from the results of the present study described below.

Fig. 9.1 shows the distribution of daily precipitation of both models averaged over the last 45-day period of the time integration. According to this comparison, the distribution of precipitation of the M-model is much less zonal than that of the NM-model, particularly in the Northern Hemisphere. For example, a zonal belt of moderate precipitation is evident in the middle latitudes of the NM-model, whereas in the M-model, it is interrupted by an area of meager precipitation over the central parts of the Eurasian and the North American continents due to the blocking effect of the Tibetan Plateau and the Rocky Mountains. Also, a belt of heavy precipitation runs in the meridional direction along the western slope of the Rocky Mountain range of the M-model. In the Southern Hemisphere of the NM-model, the subtropical dry zone of the eastern Pacific penetrates into the South American continent of the NM-model, where it is limited to the oceanic region in the M-model due to the blocking effect of the Andes Mountains. In short, the present results indicate that mountain ranges tend to increase significantly the variation of climate in the zonal direction.

## 10. Conclusions

The M-model simulates some of the essential features of the flow field in the Northern Hemisphere in January. The simulation of the flow field in the Southern Hemi-

sphere has much to be desired. Particularly, the intense surface westerlies in the middle latitudes of the Southern Hemisphere are almost missing in the M-model.

The comparison between the M-model atmosphere and the NM-model atmosphere yields the following conclusions:

1) In general, the distribution of the stationary flow field in the M-model atmosphere is more realistic than that in the NM-model atmosphere. The effects of mountains are indispensable for the successful simulation of the stationary flow field, particularly in the upper troposphere and stratosphere. On the other hand, the thermal effects seem to be important in the lower troposphere.

2) The distribution of the mean geopotential height of the isobaric surfaces in the upper troposphere of the M-model shows that the stationary trough is located in the lee of major mountain ranges such as the Tibetan Plateau and the Rocky Mountains. The trough tilts from southwest to northeast indicating the northward transport of angular momentum. The area of maximum westerlies appears to the east of the trough.

3) An intense stationary cyclone forms over the Aleutian Archipelago in the lower troposphere of both the M and NM models. This result suggests that mountains are not necessary for the formation of the Aleutian low.

4) The Tibetan Plateau is responsible for the intensification and the northward shift of the lower tropospheric anticyclone over the Eurasian continent. In other words, it plays a very important role for the maintenance of the Siberian high.

5) The M-model simulates successfully some of the qualitative features of the stationary flow in the stratosphere such as the Aleutian anticyclone and the intense trough over the North American continent. However, the intensity of the zonal wind in the model stratosphere is much stronger than the observed wind. The flow field in the NM-stratosphere appears to be more zonal and is much less realistic though it fails to reach a quasi-steady state toward the end of the time integration.

6) In the Southern Hemisphere of the M-model, the effects of mountains upon stationary disturbances are relatively small because of the lack of large-scale mountains in middle latitudes. Accordingly, the flow field tends to be more zonal than in the Northern Hemisphere.

7) The kinetic energy of stationary disturbances increases appreciably whereas that of transient eddies decreases as a result of incorporating the effects of mountains into the model. Because of these two compensating tendencies, the total eddy kinetic energy in the model troposphere is affected little by mountains.

8) A similar tendency of compensation between the stationary and transient components is evident in the northward transport of heat, angular momentum and moisture by large-scale eddies.

<sup>8</sup> See Holloway and Manabe (1971) for the detailed discussion of the distribution of precipitation in the M-model.

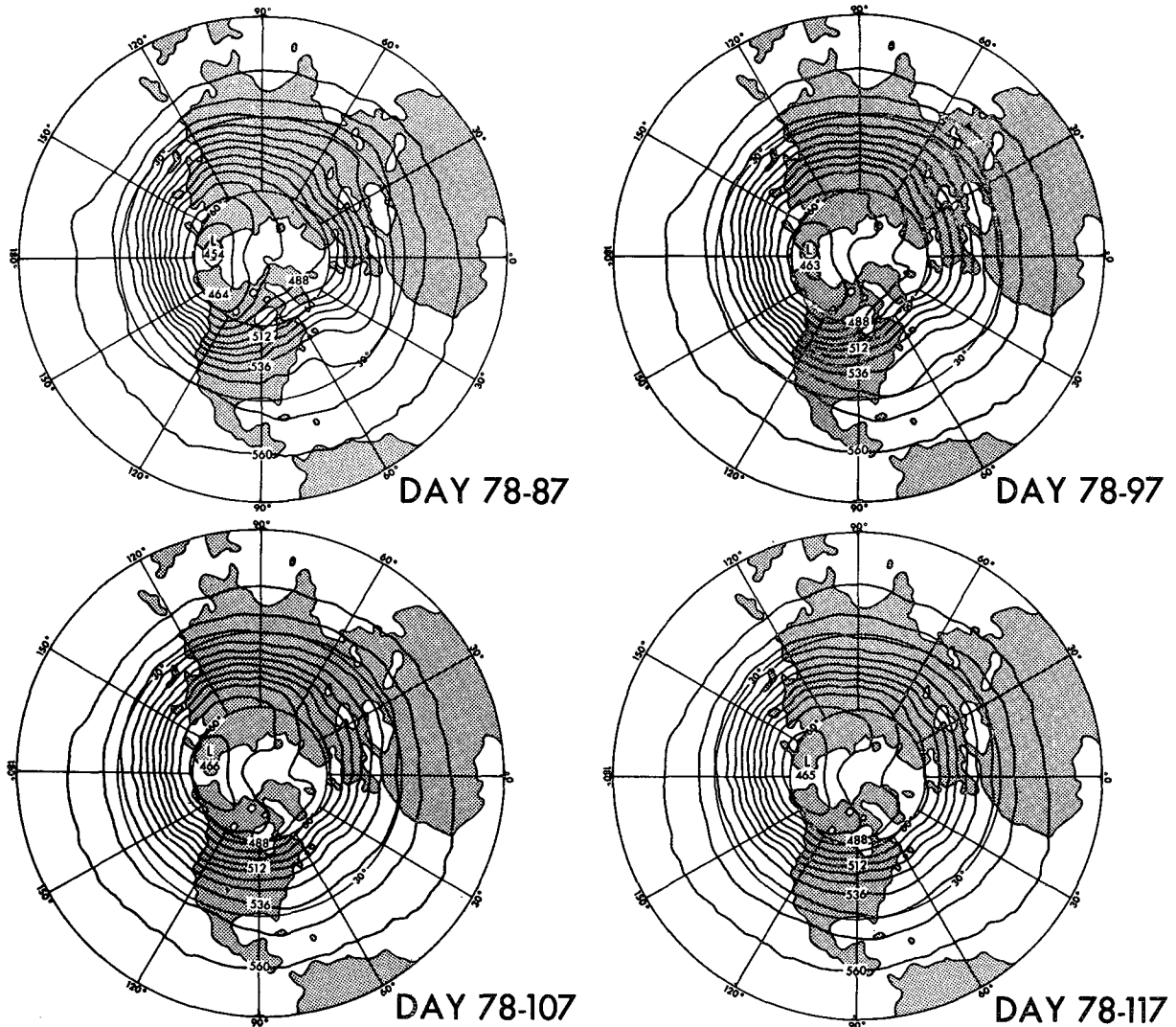


FIG. A1. Geopotential height maps of the 500-mb level of the NM-model averaged over 10-, 20-, 30- and 40-day periods: units, geopotential decameters.

9) Although mountain torque is not necessarily negligible in the budget of angular momentum in the M-model atmosphere, the latitudinal distribution of total poleward transport of angular momentum in the M-model atmosphere differs little from that of the NM-model atmosphere.

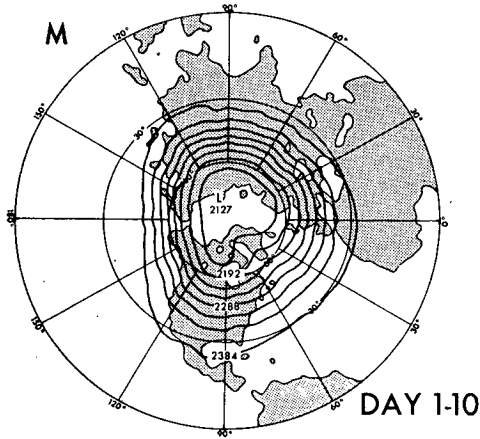
10) The conversion of potential energy into kinetic energy of stationary disturbances in the Northern Hemisphere of the model increases markedly due to the incorporation of mountain effects. This is the major reason for the increase of the kinetic energy of stationary disturbances mentioned above. Mountains, however, reduce the rate of transient eddy conversion such that the total eddy conversion in the model troposphere is hardly altered due to the effects of mountains.

11) The wavenumber analysis of total eddy conversion indicates that mountains are responsible for

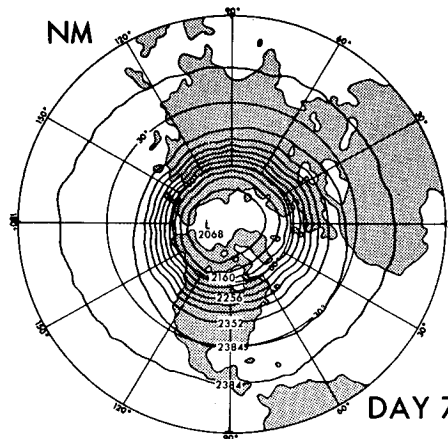
appreciably increasing the longitudinal scale of eddy conversion in the model atmosphere. This increase chiefly results from the large increase of the stationary component of eddy conversion which takes place at very low wavenumbers. It should be pointed out that the characteristic scale of the transient component of eddy conversion also increases somewhat as a result of incorporating the effects of mountains.

In response to the increase of the characteristic scale of eddy conversion mentioned above, the longitudinal scale of the disturbance also increases significantly. Again, this increase mainly results from a marked increase of the kinetic energy of stationary eddies at very low wavenumbers.

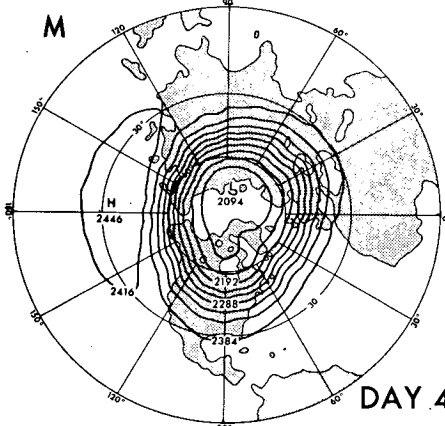
12) The energy exchange between the stratosphere and the troposphere through the stationary component of eddy pressure interaction is enhanced very much in



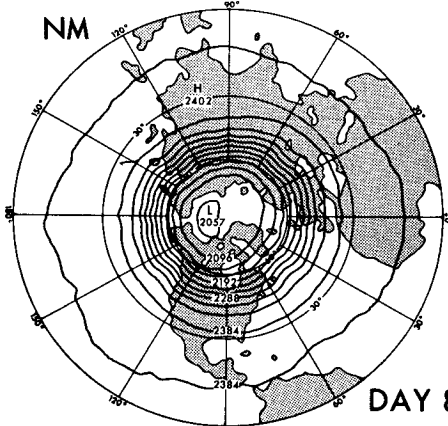
DAY 1-10



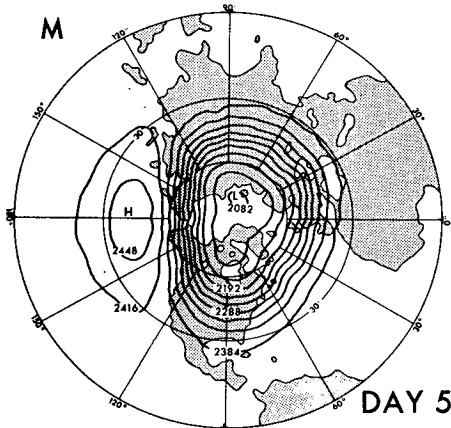
DAY 78-87



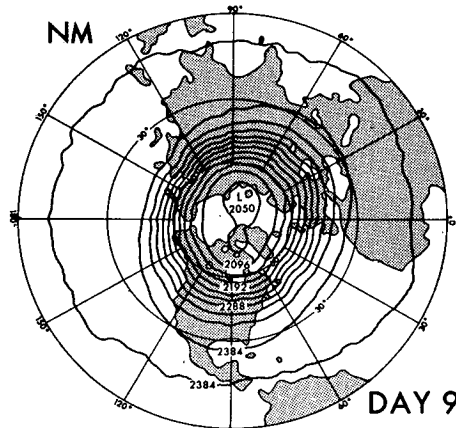
DAY 41-50



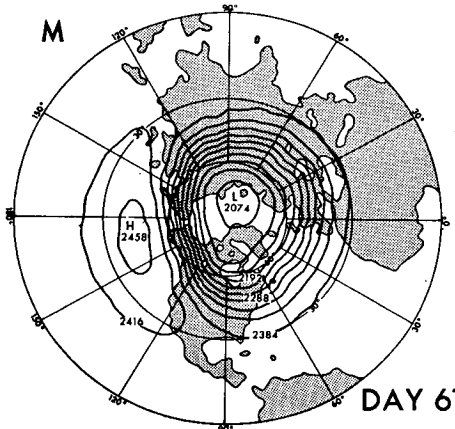
DAY 88-97



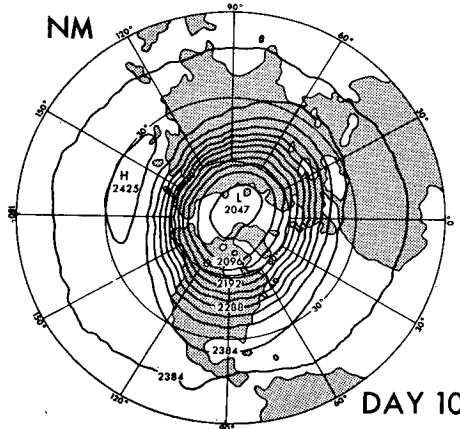
DAY 51-60



DAY 98-107



DAY 61-70



DAY 108-117

the Northern Hemisphere of the model by the effects of mountains. This is a major reason why the eddy kinetic energy of the stationary disturbances in the M-model stratosphere is much larger than that in the NM-model stratosphere. A secondary reason is the increase of stationary eddy conversion in high latitudes of the Northern Hemisphere of the model caused by the incorporation of mountain effects.

13) A major mountain range such as the Tibetan Plateau or the Rocky Mountains tends to increase the probability of cyclogenesis in the lee of the mountain range.

14) The distribution of the time-mean rate of precipitation in the M-model atmosphere is much less zonal and more realistic than that in the NM-model atmosphere.

*Acknowledgments.* The authors would like to thank Mr. J. Leith Holloway, Jr., who supervised and participated in the programming of the global model used for this study. He was also responsible for the actual execution of the numerical experiments described in this paper.

We owe very much to Dr. Abraham H. Oort who has given us much useful advice throughout the course of this study and kindly made available various observational data for this project. Particularly, he let us use the distribution of the mountain torque shown in Fig. 7.1 before its publication.

We are very grateful to Dr. Joseph Smagorinsky for his useful discussions and encouragement during the course of this project.

The authors wish to express their appreciation to Dr. Jenne of the National Center for Atmospheric Research. He kindly sent us the magnetic tape with the observed distribution of the geopotential height of isobaric surfaces shown in Figs. 4.1 and 4.9.

Thanks are due to Drs. Jerry D. Mahlman, Robert Gall and Brian Hoskins who read the paper and gave many useful comments. Finally, it is a pleasure to express gratitude to Messrs. Hank W. Moore and Philip Tunison and Mrs. Elaine D'Amico whose assistance was indispensable in the preparation of this manuscript.

APPENDIX A

Period of Time Averaging

In this study, various fundamental variables such as the flow field and the geopotential height of an isobaric surface are separated into two parts, i.e., stationary and transient. One can compute the stationary component of a field by taking the time average over a certain period of time. It is desirable that the period of time averaging chosen be long enough so that the stationary

component no longer depends upon the length of the averaging period. Such a condition is satisfied when the averaging period is longer than the time scale of most of the atmospheric disturbances.

Fig. A1 shows the geopotential height maps of the 500-mb surface of the NM-model averaged over various lengths of time. According to this figure, the time-mean distribution of geopotential height depends little upon the period of averaging if the period is longer than 30 days. Therefore, the averaging period of 40 days adopted for this study should be long enough for getting a stationary component.

Unfortunately, similar situations do not hold for the model stratosphere, where the characteristic time scale of disturbances seem to be much longer. Fig. A2 shows how a 10-day mean distribution of geopotential heights of the 30-mb level of the M-model and NM-model changes with time. The day numbers in this figure indicate the number of model days which have passed since the computational grid size is changed from about 500 km to 250 km. (The initial condition for the NM-model run is the state of the high resolution M-model atmosphere on the 60th day of its time integration). This figure shows that the distributions of geopotential height of both models (particularly the NM-model) continuously changed throughout the period of the time integrations. For example, an elongated planetary wave in the NM-model stratosphere changes into an almost circular vortex shortly after the elimination of mountains. However, the vortex elongated again toward the end of the integration of the NM-model. These results indicate that the averaging period of 40 days is too short for getting stationary disturbances in the stratosphere. Therefore, it is desirable to extend the time integration further. This was not done because of limited computer time.

APPENDIX B

Computation of Mountain Torque

The zonal component of torque exerted by mountains upon the atmosphere,  $M_1$ , may be evaluated from

$$M_1 = -a \cos\theta \overline{\left[ p_* \frac{\partial Z_*}{a \cos\theta \cdot \partial \lambda} \right]}, \tag{A1}$$

where  $a$  is the radius of the earth,  $\theta$  and  $\lambda$  are latitude and longitude,  $Z_*$  and  $p_*$  are the height and pressure of earth's surface, and the brackets and the overbar denotes the zonal and time-mean operator, respectively.

On the other hand, the mountain torque may be computed by mass-integrating the torque due to pressure gradient force throughout the entire vertical column of the atmosphere. The mountain torque thus

FIG. A2. Ten-day mean maps of geopotential height of the 30 mb-level: left, the M-model; right, the NM-model. Units: geopotential decameters.

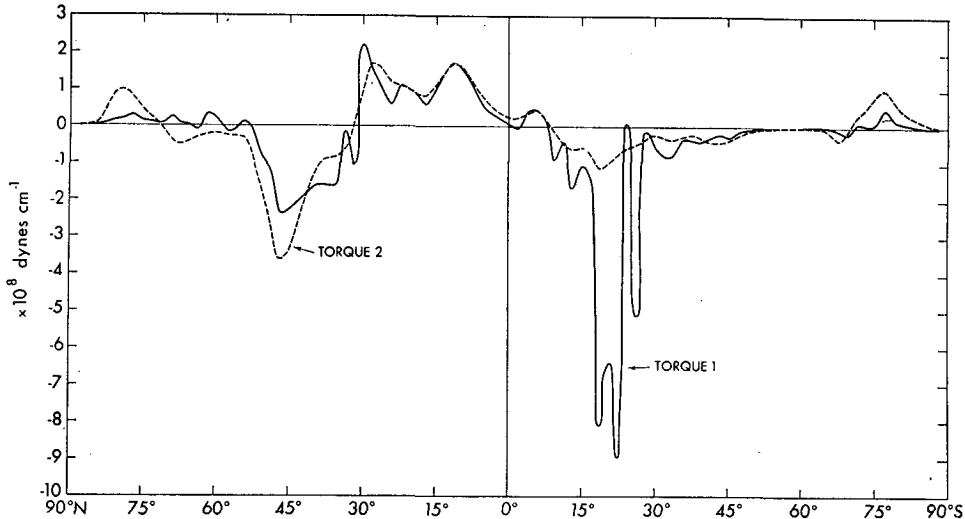


FIG. A3. The latitudinal distributions of mountain torque ( $10^8$  dyn  $\text{cm}^{-1}$ ) in the model atmosphere: solid line,  $M_1$ -torque; dashed line,  $M_2$ -torque.

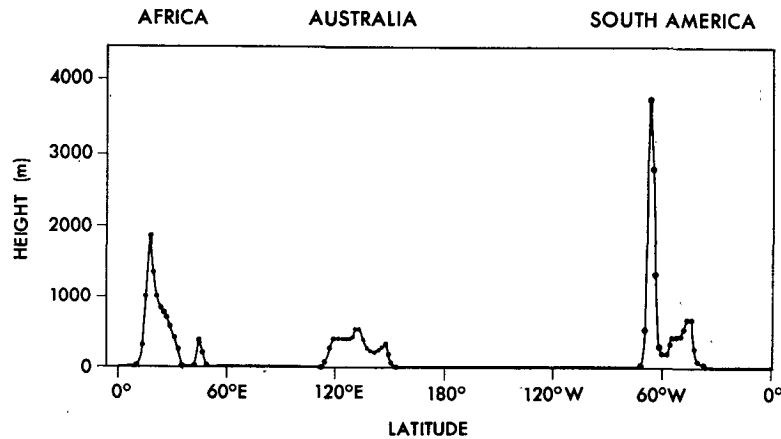


FIG. A4. The longitudinal distribution of the height  $Z_*$  of the earth's surface of the model at 22.5S. The location of a grid point in the neighborhood of a mountain is indicated by a dot.

computed is identified here as  $M_2$  and is given by

$$M_2 = -a \cos\theta \int_0^1 \left[ \left( \frac{\partial\phi}{a \cos\theta \cdot \partial\lambda} \right)_p \right] p_* d\sigma, \quad (\text{A2})$$

where  $\sigma = p/p_*$ , and  $( )_p$  indicates differentiation on the isobaric surface. For further explanation of pressure gradient force, see Holloway and Manabe (1971).

Fig. A3 shows the latitudinal distributions of mountain torque in the model atmosphere which are estimated by using these two different equations, i.e., (A1) and (A2). According to this comparison, the two distributions disagree markedly with each other in the latitude belt of the Andes Mountains. Fig. A4, which shows the longitudinal distribution of surface height  $Z_*$ , indicates that a very sharp peak of the Andes Mountains is very poorly handled by the finite-difference grid

system adopted for this study. Therefore, it is probable that the large discrepancy mentioned above is chiefly caused by the large truncation error of finite-difference computation.<sup>9</sup> As speculated in Section 4, this inconsistency in the finite-difference computation of the pressure gradient force may be partly responsible for the unrealistic features of the sea level pressure in the neighborhood of steep topography such as Antarctica or Greenland. Further improvement of the computation of the pressure gradient force is desirable.

The latitudinal distribution of mountain torque, which is discussed in Section 7, represents  $M_2$ , i.e., the

<sup>9</sup> Because of the limited length of computer time available toward the end of this project,  $M_2$  was computed by use of data taken with the interval of 48 hr rather than 24 hr. Therefore, the difference between  $M_1$  and  $M_2$  may partly be due to the sampling error. The magnitude discrepancy in the latitude belt of the Andes Mountains is too large to be explained by this cause.

mountain torque experienced by the model atmosphere rather than the torque exerted by mountain surface. As one would expect, the balance requirement of angular momentum in the model atmosphere is satisfied better by choosing  $M_2$ -torque rather than  $M_1$ -torque.

## REFERENCES

- Bolin, B., 1950: On the influence of the earth's orography on the general character of the westerlies. *Tellus*, **2**, 184-195.
- Budyko M. I., Ed., 1963: *Atlas Teploogo Balansa Zemnogo Shara* (Guide to the Atlas of the Heat Balance of the Earth). Moscow, Gidrometeoizdat, 69 pp.
- Charney, J. G., and A. Eliassen, 1949: A numerical method for predicting the perturbations of the middle latitude westerlies. *Tellus*, **1**, 38-54.
- , and J. Pedlosky, 1963: On the trapping of unstable planetary waves in the atmosphere. *J. Geophys. Res.*, **68**, 6441-6442.
- Döös, B. R., 1962: The influence of exchange of sensible heat with the earth's surface on the planetary flow. *Tellus*, **14**, 133-147.
- Dopplück, T. G., 1971: The energetics of the lower stratosphere including radiative effects. *Quart. J. Roy. Meteor. Soc.*, **97**, 209-237.
- Holloway, J. L., Jr., and S. Manabe, 1971: Simulation of climate by a global general circulation model: I. Hydrologic cycle and heat balance. *Mon. Wea. Rev.*, **99**, 335-370.
- , M. J. Spelman and S. Manabe, 1973: Latitude-longitude grid suitable for numerical time integration of a global atmosphere model. *Mon. Wea. Rev.*, **101**, 69-78.
- Holopainen, E. O., 1970: An observational study of the energy balance of the stationary disturbances in the atmosphere. *Quart. J. Roy. Meteor. Soc.*, **96**, 626-644.
- Hydrographic Office, U. S. Navy, 1944: *World Atlas of Sea Surface Temperature*, 2nd ed. H. O. Publ. No. 225.
- , 1964: *World Atlas of Sea Surface Temperature*, 2nd ed. H. O. Publ. No. 225 with supplements.
- Kasahara, A., and W. M. Washington, 1969: Thermal and dynamical effects of orography on the general circulation of the atmosphere. *Proc. WMO/IUGG Symp. Numerical Weather Prediction*, Tokyo, Japan Meteor. Agency, IV 47-IV 56.
- , and —, 1971: General circulation experiments with a six-layer NCAR model, including orography, cloudiness, and surface temperature calculations. *J. Atmos. Sci.*, **28**, 657-701.
- Kikuchi, Y., 1969: Numerical simulation of the blocking process. *J. Meteor. Soc. Japan*, Ser. 2, **47**, 29-54.
- Kurihara, Y., and J. L. Holloway, Jr., 1967: Numerical integration of a nine-level global primitive equations model formulated by the box method. *Mon. Wea. Rev.*, **95**, 509-530.
- Mahlman, J. D., 1969: Energetics of a "minor breakdown" of the stratospheric polar night vortex. *J. Atmos. Sci.*, **26**, 1306-1317.
- Manabe, S., 1969: Climate and ocean circulation: 1. The atmospheric circulation and the hydrology of the earth's surface. *Mon. Wea. Rev.*, **97**, 739-774.
- , and D. G. Hahn, 1974: The seasonal variation of the stratospheric circulation as simulated by a global model of the atmosphere. (To be published.)
- , and J. L. Holloway, Jr., 1970: Climate modification and a mathematical model of atmospheric circulation. *A Century of Weather Progress*, Boston, Amer. Meteor. Soc., 157-164.
- , —, and H. M. Stone, 1970a: Tropical circulation in a time integration of a global model of the atmosphere. *J. Atmos. Sci.*, **27**, 580-613.
- , J. Smagorinsky, J. L. Holloway, Jr. and H. M. Stone, 1970b: Simulated climatology of a general circulation model with a hydrologic cycle. III. Effects of increased horizontal computational resolution. *Mon. Wea. Rev.*, **98**, 175-212.
- , —, and R. F. Strickler, 1965: Simulated climatology of a general circulation model with a hydrologic cycle. *Mon. Wea. Rev.*, **93**, 769-798.
- , and R. F. Strickler, 1964: Thermal equilibrium of the atmosphere with convective adjustment. *J. Atmos. Sci.*, **21**, 361-385.
- , and R. T. Wetherald, 1967: Thermal equilibrium of the atmosphere with a given distribution of relative humidity. *J. Atmos. Sci.*, **24**, 241-259.
- Mintz, Y., 1965: Very long-term global integration of the primitive equations of atmospheric motion. WMO Tech. Note No. 66, 141-167.
- Miyakoda, K., 1963: Some characteristic features of winter circulation in the troposphere and lower stratosphere. Tech. Rept. No. 14, Grant NSF-GP-471, Dept. of Geophysical Sciences, The University of Chicago, 93 pp.
- , G. D. Hembree, R. F. Strickler and I. Shulman, 1972: Cumulative results of extended forecast experiments: 1. Model performance for winter cases. *Mon. Wea. Rev.*, **100**, 836-855.
- Möller, F., 1951: Vieteljahrs Kanten des Niederschlags für die Ganze Erde. *Petermanns Geograph. Mill.*, **95**, 1-7.
- Newell, R. E., D. G. Vincent, T. G. Dopplück, D. Ferruzza and J. W. Kidson, 1971: The energy balance of the global atmosphere. *Proc. London Conference on General Circulation*, Roy. Meteor. Soc., 42-90.
- Newton, C. W., 1956: Mechanisms of circulation change during a lee cyclogenesis. *J. Meteor.*, **13**, 528-539.
- , 1971: Global angular momentum balance: Earth torques and atmospheric fluxes. *J. Atmos. Sci.*, **28**, 1329-1341.
- Oort, A. H., 1964: On the energetics of the mean and eddy circulations in the lower stratosphere. *Tellus*, **16**, 309-327.
- , and H. D. Bowman II, 1974: A study of the mountain torque. To be submitted.
- , and E. M. Rasmusson, 1971: Atmospheric circulation statistics. NOAA Prof. Paper 5, Govt. Printing Office, Washington, D. C., 323 pp.
- Petterssen, S., 1956: *Weather Analysis and Forecasting*, Vol. 2. New York, McGraw-Hill, 266 pp.
- Phillips, N. A., 1956: The general circulation of the atmosphere: A numerical experiment. *Quart. J. Roy. Meteor. Soc.*, **82**, 123-164.
- , 1957: A coordinate system having some special advantages for numerical forecasting. *J. Meteor.*, **14**, 184-185.
- Reed, R. J., J. L. Wolfe and H. Nishimoto, 1963: A spectral analysis of the energetics of the stratospheric sudden warming of early 1957. *J. Atmos. Sci.*, **20**, 256-275.
- Saltzman, B., 1968: Surface boundary effects on the general circulation and macroclimate: A review of the theory of the quasi-stationary perturbations in the atmosphere. *Meteor. Monogr.*, **8**, No. 30, 4-19.
- , and A. Fleisher, 1961: Further statistics on the modes of release of available potential energy. *J. Geophys. Res.*, **66**, 2271-2273.
- Sankar-Rao, M., 1965: Continental elevation influence on the stationary harmonics of the atmosphere motion. *Pure Appl. Geophys.*, **60**, 141-159.
- , 1970: On global monsoons—further results. *Tellus*, **22**, 648-654.
- , and B. Saltzman, 1969: On a steady-state theory of global monsoons. *Tellus*, **21**, 308-330.
- Smagorinsky, J., 1953: The dynamical influence of large-scale heat sources and sinks on the quasi-stationary mean motions of the atmosphere. *Quart. J. Roy. Meteor. Soc.*, **79**, 342-366.
- , 1963: General circulation experiments with the primitive equations. *Mon. Wea. Rev.*, **91**, 99-164.
- Taljaard, J. J., H. van Loon, H. L. Crutcher and R. L. Jenne, 1969: *Climate of the Upper Air, Part I—Southern Hemisphere: Vol. 1, Temperatures, Dew Points, and Heights at Selected*

*Pressure Levels*. NAVAIR 50-1C-55 (available from Naval Weather Service Command, Washington Navy Yard, Washington, D. C.).

Washington, W. M., 1973: Development of a three-dimensional stratospheric global circulation model at the National Center for Atmospheric Research. *Proc. Second Conference on CIAP*, U. S. Dept. of Transportation, 358-362.

—, and A. Kasahara, 1970: A January simulation experiment with the two-layer version of the NCAR global circulation model. *Mon. Wea. Rev.*, **98**, 559-580.

White, R. M., 1954: The countergradient flux of sensible heat in the lower stratosphere. *Tellus*, **6**, 177-179.

Widger, W. K., Jr., 1949: A study of the flow of angular momentum in the atmosphere. *J. Meteor.*, **6**, 291-299.